Detection and Removal of Hyper-synchronous Artifacts in Massively Parallel Spike Recordings

Jonas Oberste-Frielinghaus[1,2*], Aitor Morales-Gregorio[1], Simon Essink[1,2], Alexander Kleinjohann[1,2], Sonja Grün[1,3], Junji Ito[1]

January 11, 2024

[1]Institute of Neuroscience and Medicine (INM-6) and Institute for Advanced Simulation (IAS-6) and JARA-Institute Brain Structure-Function Relationships (INM-10), Jülich Research Centre, Jülich, Germany
[2]RWTH Aachen University, Aachen, Germany
[3]Theoretical Systems Neurobiology, RWTH Aachen University, [Worringerweg 3, 52056] Aachen, Germany
[*]Correspondence: j.oberste-frielinghaus@fz-juelich.de

Summary

Current electrophysiology experiments often involve massively parallel recordings of neuronal activity using multi-electrode arrays. While researchers have been aware of artifacts arising from electric cross-talk between channels in setups for such recordings, systematic and quantitative assessment of the effects of those artifacts on the data quality has never been reported. Here we present, based on examination of electrophysiology recordings from multiple laboratories, that multielectrode recordings of spiking activity commonly contain extremely precise (at the data sampling resolution) spike coincidences far above the chance level. We derive, through modeling of the electric cross-talk, a systematic relation between the amount of such hyper-synchronous events (HSEs) in channel pairs and the correlation between the raw signals of those channels in the multi-unit activity frequency range (250-7500 Hz). Based on that relation, we propose a method to identify and exclude specific channels to remove artifactual HSEs from the data. We further demonstrate that the artifactual HSEs can severely affect various types of analyses on spike train data. Taken together, our results warn researchers to pay considerable attention to the presence of HSEs in spike train data and to make efforts to remove the artifactual ones from the data to avoid false results.

Introduction

Modern electrophysiological experiments often use multi-electrodes, such as Utah arrays (Blackrock Microsystems, Salt Lake City, UT, USA) (de Haan et al., 2018; Chen et al., 2022) and Neuropixels probes (Cambridge NeuroTech, Cambridge UK) (Jun et al., 2017), to record neuronal activity at multiple sites simultaneously. The number of recording channels has been constantly increasing owing to incremental improvements in both hardware and software systems (Stevenson & Kording, 2011). However, these recordings are known to be very sensitive to internal and external noise (Rey et al., 2015; Harris et al., 2016), which need to be mitigated to enable reliable and robust data analysis. In particular, multi-electrode recordings are highly sensitive to cross-talk between channels, an often ignored problem in systems neuroscience.

Signal artifacts are known to appear in neural recordings due to noise from both internal (muscle movements, heartbeats, eye movements, chewing etc.) and external (electric grid interference, loud noises etc.) sources (Fabietti et al., 2020). All these sources are of non-neural origin, and can often be distinguished from neural activity owing to their particular frequencies and distinct waveforms. Removal methods are often based on Independent Component Analysis (ICA) (Bell & Sejnowski, 1995; Rong & Contreras-Vidal, 2006; Delorme et al., 2007), Canonical Correlation Analysis (CCA) (Hotelling, 1936; Wim De Clercq et al., 2006), Wavelet methods, or certain combinations thereof. These are often applied to Electroencephalogram (EEG) (Wim De Clercq et al., 2006; Delorme et al., 2007; Shackman et al., 2009; Barban et al., 2021; Mumtaz et al., 2021) and Magnetoencephalogram (MEG) (Rong & Contreras-Vidal, 2006) data, and to a lesser extent also to extracellular electrophysiology (Ludwig et al., 2009; Islam et al., 2014; Fabietti et al., 2020).

Besides common noise sources, capacitive coupling between shanks or cables can cause cross-talk between different channels (Nelson et al., 2017), leading to a mixing of neural signals that can persist even after spike sorting (Torre et al., 2013). Cross-talk is a well-known problem in EEG (Nagaoka et al., 1992) and electromyogram (EMG) (Koh & Grabiner (1993); Kilner et al. (2002); Farina et al. (2004)) data recording systems. However, to the best of our knowledge, only a few studies have focused on cross-talk in electrophysiology systems (Musial et al., 2002; Nelson et al., 2017; Pérez-Prieto & Delgado-Restituto, 2021).

Extremely precise (within $\frac{1}{30}$ ms) synchronous spiking events have been linked to cross-talk artifacts (Yu et al., 2009; Torre et al., 2013; Dehnen et al., 2021; Chen et al., 2022), since they occur well above the expectation from chance coincidences of spikes. Spiking activity is known to be coordinated on the timescales of a few milliseconds (König et al., 1995; Riehle et al., 1997; Butts et al., 2007; Grün, 2009), but no observation of sub-millisecond coordination has ever been reported, nor are there any known mechanisms that would enable sub-millisecond synchronization. Furthermore, the separation between electrodes in those studies was $\geq 400\ \mu$m, well beyond the spatial reach of extracellular electrodes (Henze et al., 2000), denying the possibility that the apparent sub-millisecond synchronization is merely an identical spike recorded by multiple electrodes. Therefore, these sub-millisecond precision synchronous events were considered artifacts, which we name here *synchrofacts* (short for synchronous artifacts).

Several methods have been suggested to remove the synchrofacts from neural recordings. Hardware implementations can avoid cross-talk by improving the isolation and design of the circuits (Blot & Barbour, 2014; Nelson et al., 2017; Pérez-Prieto & Delgado-Restituto, 2021; Perez-Prieto et al., 2021). Most neuroscientists do not design their own custom hardware, and hence have to use post-hoc methods to remove the synchrofacts from their data. Some studies remove certain spikes from further analysis (Musial et al., 2002; Torre et al., 2013; Dann et al., 2016; Dehnen et al., 2021), either during the spike sorting process (Musial et al., 2002; Dann et al., 2016) or post-hoc (Torre et al., 2013; Dehnen et al., 2021). Removing individual spikes can be very sensitive to the specific selected criteria and might require manual verification that the removal worked as intended. Other studies remove entire channels or neurons instead (Churchland et al., 2006; Yu et al., 2009; Snyder et al., 2021; Chen et al., 2022; Semedo et al., 2022; Morales-Gregorio et al., 2023), since not all channels are equally affected by synchrofacts (Chen et al., 2022). This

approach also mitigates artifacts in continuous signals. However, most removal methods are relatively complex, computationally expensive, and might require manual verification of the results.

To overcome the limitations of the above mentioned methods, we here show that cross-talking channels can be detected from both the raw signal cross-correlation and threshold crossing synchrony. Our detection method is tested on two extracellular electrophysiology data sets of recordings from macaque monkeys from two different experimental laboratories (de Haan et al., 2018; Chen et al., 2022). A theoretical model confirms that the experimental observations are consistent with what is expected from cross-talk between recording channels. Furthermore, we propose and evaluate several methods to remove synchrofacts based on our metrics. Finally, we demonstrate that the presence of synchrofacts can radically affect analysis results, such that false results will emerge. We will demonstrate that on a) neuronal tuning curves and on b) the results from the Unitary Event analysis (Grün et al., 1999, 2002a,b; Grün, 2009), which detects excess spike synchrony. The application examples highlight the need for the detection and the removal of synchrofacts. All in all, our methods construe a novel and simple approach to cross-talk detection and synchrofact removal that can be applied to any multi-electrode recording system, to ensure cleaner and more reliable data.

Results

Synchronous spike events are ubiquitous in multi-electrode systems

One focus of our interest in the analysis of massively parallel spike train data lies on fine-temporal correlations in the spiking activity of a population. As an initial analysis step for such an examination (and to detect potential artifacts), we inspect the dot-display of the simultaneously recorded spike trains.(Figure 1b, top), here shown for two different data sets from two different laboratories and monkeys (Figure 1a). Therein we notice events in which seemingly many neurons exhibit spike-like events simultaneously (Figure 1b, highlighted in gray). To further investigate this observation, we compute the population spike time histograms with different bin sizes to evaluate spike correlations on different time scales. At the resolutions of 1ms and $\frac{1}{30}$ ms, we find some bins with outstandingly high spike counts, which were not visible at the resolution of 10 ms. Whereas neurons can coordinate their activity with millisecond precision (König et al., 1995; Riehle et al., 1997; Butts et al., 2007), to the best of our knowledge, synchronization on the $\frac{1}{30}$ ms time scale has never been reported in neuronal activity, and there is no known neural mechanisms that could produce it. We term these surprisingly precise spike coincidences as hyper-synchronous events (HSEs).

To study whether the observed amount of HSEs can be explained by chance coincidences of spikes, we quantify the HSEs by their complexity (i.e., number of involved neurons) (Grün et al., 2008) and compare them to the complexities expected by chance using a surrogate method (Stella et al., 2022). Here we generate 200 surrogate data sets by time-shifting each spike train by a shift size independently drawn from a uniform distribution between 0 and and 30ms (Figure 1c). Time shifting destroys potential correlations between spike trains, while conserving many other features of the data such as the inter-spike interval distribution, the firing rate modulations and autocorrelation (Stella et al., 2022).

Figure 1d shows the complexity distributions of the original and the surrogate data, for two different bin widths (1 ms and $\frac{1}{30}$ ms). We find that, for the both bin width, high complexity events occur much more often in the original data than in the surrogate data. Particularly, with $\frac{1}{30}$ ms bin width (Figure 1d, bottom), we find in the original data complexities up to 10 (macaque Y) or 13 (macaque L), but in the surrogate data complexities only up to 6 or 7, respectively. Thus, fine temporal synchrony by chance occurs much less than what we observe in the experimental data, indicating that many of the HSEs in the experimental data might not originate from neuronal activity. Furthermore, the literature (e.g. Shu et al. (2007)) did not report on cortical action potentials shorter than 1 ms. Considering all these findings, we conclude that the observed excess synchronous events are artifacts.

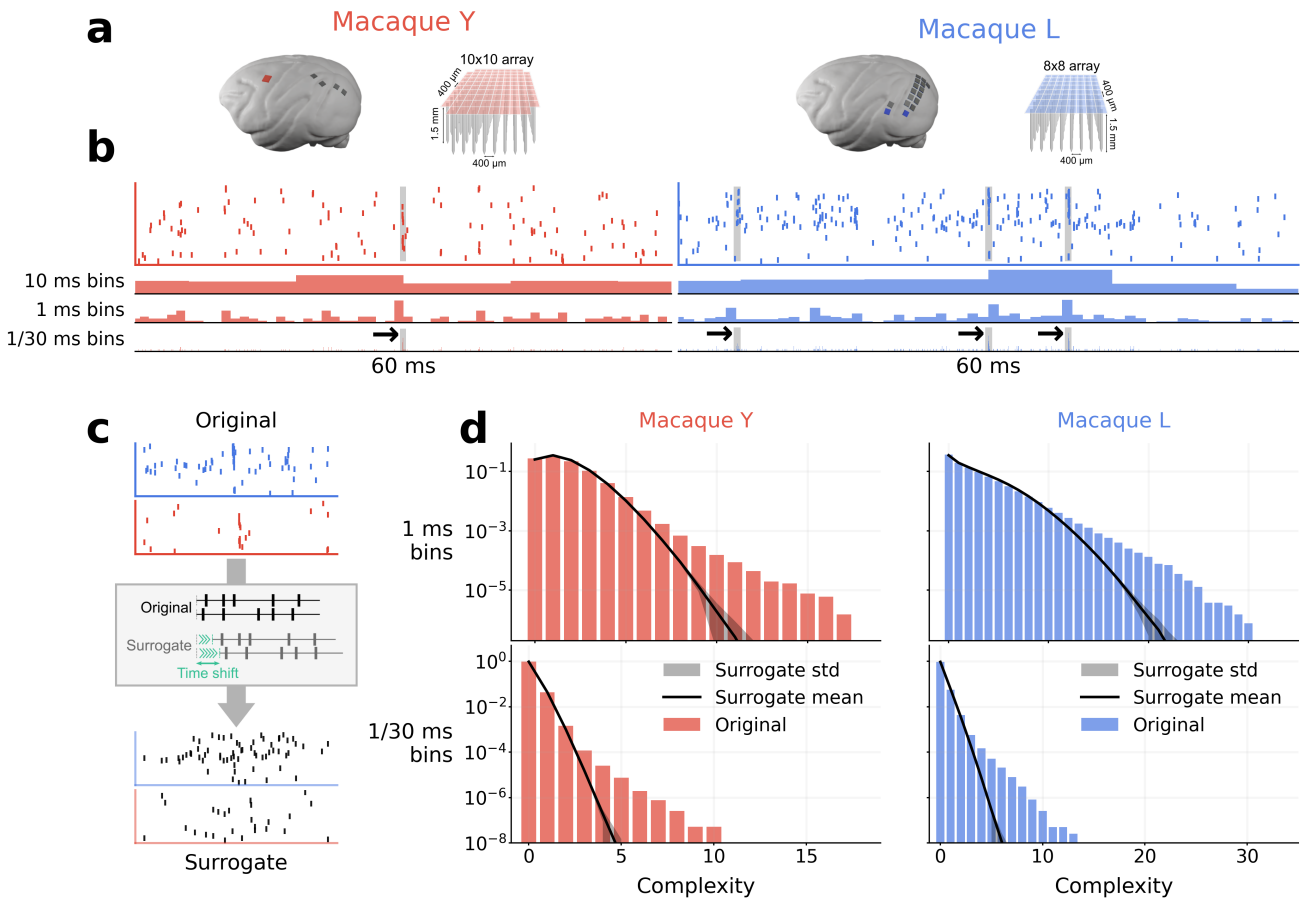

Figure 1: Observation of hyper-synchronous event (HSEs). (a) Electrode arrays and implantation sites for the two macaques, macaque Y: 6x6 electrode arrays in V1, V2, DP, 7A and 10x10 in M1/PMd, but we focus here only on the 10x10 array; macaque L: 14 8x8 arrays in V1 and two in V4 with the focus here on an array pair with one in V1 and one in V4. The arrays focused on are colored. (b) Dot display (top) and population histograms with different bin sizes (bottom) for a 60 ms long data slice. HSEs are highlighted with gray. (c) Illustration of the surrogate generation to generate independent data. Original spike trains are shifted against each other by a random amount of time. (d) Complexity distribution of the original data (colored bars), and the mean and standard deviation (line and shade, respectively) for the complexity distribution of the respective surrogates; top with 1 ms bin size, bottom with $\frac{1}{30}$ ms bin size.

This type of artifact, which we name synchrofacts, can only be spotted when analyzing the spiking activity on very fine time scales and shows itself in an excess of HSEs.

We find synchrofacts in two separate setups for massively parallel electrophysiological recordings (both using the Blackrock recording system) originating from two different laboratories and recorded in two different monkeys. Therefore we suspect that synchrofacts are common across recordings of the same type, but we also know that they occur in other recording systems, e.g. in Neuropixel recordings (Jain et al., 2022). Taken together, our observations and previous reports highlight the ubiquity of synchrofacts.

Simply removing all HSEs from the data is not an appropriate solution to get rid of the synchrofacts, since this would also remove many genuine neuronal spikes and neural synchrony. We can demonstrate this by removing all spikes in the bins with complexity of two or larger at $\frac{1}{30}$ ms resolution, and then calculating the complexity distribution, to compare it to the surrogate complexity distribution. In the surrogate distribution we see complexities of two or higher occurring by chance (Figure 1d). However, since this way all synchronous spikes from the original data are removed, the original distribution totally lacks complexities higher than 2, and hence it differs vastly from the surrogate distribution (see Supplementary Figure S1). Thus, removing all HSEs alters the statistic properties of the spike trains significantly, and is not applicable if we do not want to influence our analysis methods.

We see on the one hand the need for removing all synchrofacts from the data to perform proper analyses, but on the other hand we need to take care not to exclude neuronal spike synchrony in order to retain the correct chance correlation level even on a lower time resolution, e.g., 1 ms. Thus, we aim at selectively removing synchrofacts from the data, and to this end, we need to discriminate synchrofacts from chance coincidences of real spikes.

Synchronous spike events with nearly identical raw signals are not of neural origin

Following the observations in the previous sections, we now take a deeper look at the HSEs to see if synchrofacts can be discriminated from chance spike coincidences. As discussed before, we expect a certain amount of HSEs of some complexities to occur by chance. Hence, whereas a HSE with a very high complexity would be most likely to be a synchrofact, we cannot completely rule out the possibility that it is a real spike synchrony that occurred by chance. Thus, we have no way of discriminating between synchrofacts and real spike synchrony as long as we examine them only on the description level of spikes. We need to take additional information into account to spot if a HSE is a synchrofact. To this end, we inspect the raw signals from which the spike events are extracted, and look there for features characterizing synchrofacts.

We extracted putative spikes by thresholding the band-pass filtered raw signals in the frequency range of 250 Hz – 7500 Hz (see Signal processing and threshold crossings in Methods for details). For simplicity, we henceforth refer to the band-pass filtered raw signal merely as raw signal, unless noted otherwise. We plot the raw signals of multiple channels around the timing of one HSE (Figure 2a) and observe that indeed highly similar spike-like waveforms are present on multiple different electrodes simultaneously, but with different amplitudes. Furthermore, even the ongoing signal fluctuations before and after the HSE appear to be correlated across these channels. The affected channels are not necessarily in close spatial proximity, as shown in Figure 2b for one example synchrofact. We measured the distance between electrodes for all HSEs with high complexities, which are highly likely to be synchrofacts based on our surrogate analysis (Figure 1). We observed that they often involve electrodes that are far apart, up to several millimeters (Figure 2c). In particular, in the case of macaque L, HSEs appear even across the two arrays which are separated by the lunate sulcus.

To summarize, we observed sub-millisecond synchronization of spikes across channels, the nearly identical waveforms of those spikes, the visible correlation between raw signals, and the large distance between the participating electrodes. Taken together, these observations strongly suggest that many of these events are artifacts due to electric cross-talk, which could happen at multiple positions in the setup (electrode shanks, transmission cables, multiplexer etc.) in the recording apparatus, rather than multiple electrodes recording the same neuron nor some

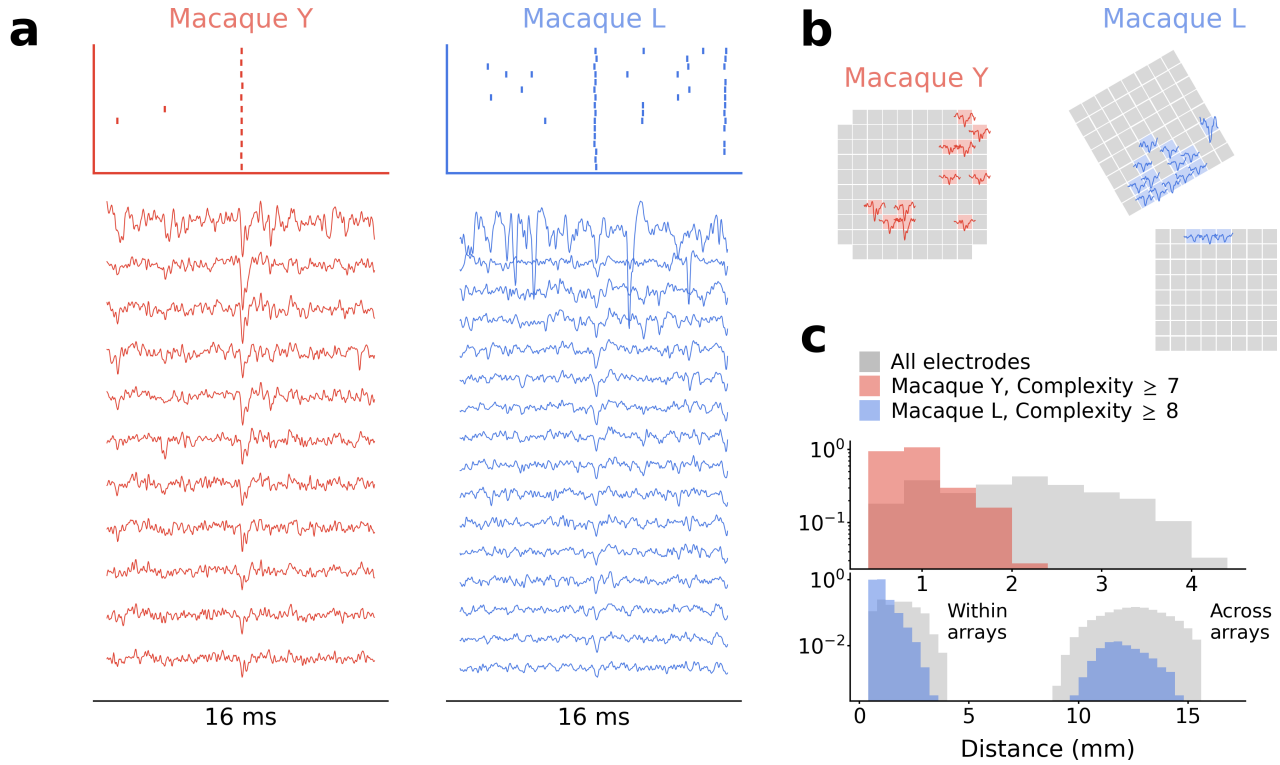

Figure 2: HSEs in relation to the raw signals for the data set of macaque Y (red) and L (blue). (a) Dot display (top) centered around a single HSE and the corresponding band-pass filtered (250 Hz - 7500 Hz) raw signals of the channels participating in the HSE. In all parallel raw signals we observe a spike-like excursion aligned on the HSE. (b) Positions of the electrodes on the respective array for the raw signal channels that take part in the HSE from panel (a). The trace of the spike-like excursion in each channel is shown at the corresponding position. (c) Distances between the electrodes that are involved in all HSEs with high complexity, selected based on the surrogate analysis from Figure 1 such that all considered HSEs are most likely synchrofacts. For reference, the distance distribution between all electrodes is shown in gray.

novel form of fast neuronal synchronization.

Cross-correlation and hyper-synchronous events can detect synchrofacts

The degree of the potential cross-talk can be quantified by calculating the Pearson correlation coefficient $c_{i,j}$ of the raw signals for each pair of channels i and j (see Cross-correlation of high-pass filtered raw signals in Methods for details). We show in Figure 3a the raw signal correlation coefficient $c_{i,j}$ between channels i and j (for $i \neq j$) in a matrix form, and in Figure 3b the distribution of the $c_{i,j}$ values in the matrix. The coefficients are generally larger than zero, i.e., the raw signals are positively correlated. The coefficient values vary strongly across channel pairs, with some pairs showing quite large correlation coefficients. These strong correlations are observed in both recording setups from different laboratories. Thus we suspect that the occurrence of such correlations is a general phenomenon in massively parallel electrophysiological recordings that use the same type of electrodes, but as will be discussed (in the Discussion) these occur also in other setups.

There may be multiple possible origins for such strong correlations in the raw signals, ranging from damages on the electrodes to electric shortcuts between channels due to various reasons, such as crossing of the implanted cables below the skull, dirt in the headstage connector, interference between the cables connected to the amplifier, and so on (see also Yu et al. (2009)). As shown in Figure 2b and c, the artifacts are not limited to spatially proximal channels but extend over the whole array or even across arrays, indicating that a deficit in a local group of channels cannot be the primary reason for these (strong) correlations. Another possibility is a local deficit on the headstage connector, but this is also denied by examining the spatial extent of correlated channels mapped on the connector (see Macaque L data in Supplementary Figure S2). Thus, there is no single reason for the observed correlations, but rather there seem to be multiple causes residing on different stages of the setup. Eliminating all possible causes from the setup is practically not feasible, and hence we cannot avoid having such correlations at least in a part of all possible channel pairs.

Excluding the channels with strong correlations from the analysis would be easy if their correlation coefficients were distinctly different from the other channels. However, as shown in Figure 3b, the distribution of the correlation coefficient values across channel pairs typically shows a smooth decay towards high values, indicating no clear critical correlation coefficient value above which the respective channel pairs are considered to be problematic. In the following we examine how an appropriate value for such a critical correlation can be derived from the relation between the raw signal correlation and the spike coincidences extracted from the raw signals.

For channel pairs with a large correlation coefficient, their raw signals are similar to each other, and hence, if one channel of such a pair had spike-like waveforms, the other channel should also have these at the same timings with similar waveforms. This leads to the expectation that synchrofacts should occur more often in a channel pair with a larger $c_{i,j}$. To confirm this, we first count, for each channel pair, the amount of HSEs (on the sampling rate resolution) which contain spikes from that pair. Based on this count we define the pairwise HSE index $I_{i,j}$ of channels i and j as the fraction of the HSE count to the minimum of the total spike counts of these two channels (see Measure of spike synchrony in Methods for the formula). We choose to divide by the smaller count so that the HSE index is independent of the channel order (i.e., $I_{i,j} = I_{j,i}$) and also sensitive to HSEs occurring on channels with small number of spikes. We show in Figure 3c the HSE index $I_{i,j}$ between channels i and j (for $i \neq j$) in a matrix form, and in Figure 3d the distribution of the $I_{i,j}$ values in the matrix. We find $I_{i,j}$ values ranging from zero to ~ 0.5, while the value excepted from an independent pair of spike trains is of order of magnitude $\sim 10^{-3}$ (see Supplementary Figure S3).

We then plot $I_{i,j}$ against the correlation coefficients c_{ij}, and examine if there is a systematic relation between these two measures. Figure 3e shows the HSE index values for all channel pairs plotted against the respective correlation coefficients $c_{i,j}$. Here we see that a majority of channel pairs have HSE index values close to zero, meaning hardly any spikes are shared by these pairs. Especially the channel pairs with low correlation coefficients $c_{i,j}$ such as < 0.2

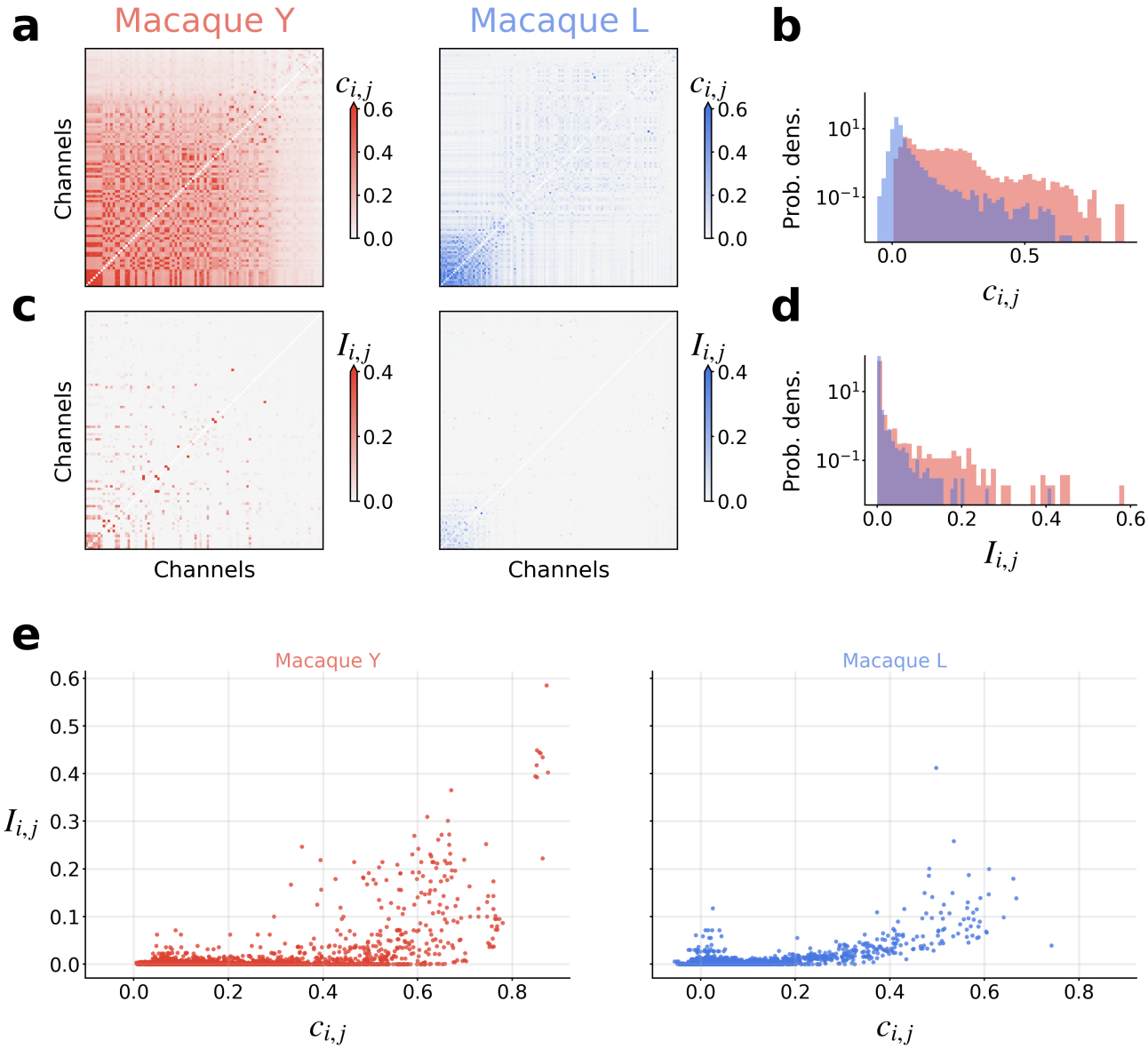

Figure 3: Relation of pairwise raw signal correlations to respective pairwise occurrences of HSEs. (a) Pairwise correlation coefficients $c_{i,j}$ of the raw signals. Data are shown in matrix form, the channels were sorted by largest maximum correlation. (b) Distribution of the $c_{i,j}$ values that appear in the matrix shown in (a). (c) HSE index $I_{i,j}$ for all channel pairs shown in a channel-by-channel matrix form. The channels are sorted in the same order as in (a). (d) Distribution of the $I_{i,j}$ values that appear in the matrix shown in (c). (e) Scatter plot of the raw signal correlation coefficient $c_{i,j}$ against HSE index $I_{i,j}$ of the corresponding channel pair, each dot represents one channel pair. Higher $I_{i,j}$ occur at higher $c_{i,j}$, common trend for both data sets

have very low HSE index values. The pairs with coefficients between 0.2 and 0.4 have slightly larger, but still quite small HSE index values. As the correlation $c_{i,j}$ gets larger than 0.4, the HSE index value rapidly increases, indicating a critical threshold for the correlation at which spikes becomes very likely to be detected on both electrodes.

We want to stress here again the difference between HSEs and synchrofacts. HSEs denote all events when two or more spikes are recorded across multiple channels simultaneously, whereas synchrofacts are only a part of the HSEs that are not chance spike coincidences. When calculating the complexity distribution (Figure 1d) we notice that a certain amount of the HSEs can be explained by chance. Therefore, a HSE index larger than zero does not immediately indicate synchrofacts. However, as we mentioned above, the HSE index expected from independent spike trains is very small, on the order of 10^{-3}. An HSE index excessively greater than this strongly indicates presence of synchrofacts.

Cross-talk model explains the emergence of synchrofacts

In the following we formulate a model to understand how the observed relation between the band pass filtered raw signal correlation and the spike event correlation index can be explained. Our previous examination of raw signals of the channels that exhibit HSE spikes confirmed that the waveforms of those spike-like events are highly similar across channels besides their amplitudes (see Figure 2a). This may imply that those spike-like events are due to an electric cross-talk. For the model we assume that this cross-talk is only an ohmic interaction (i.e., no phase shifts between the channels), such that spikes (as well as any signal deflections) that occur in one channel "bleed" into the other channels without a delay but with a certain amplitude reduction. According to this observation, here we attempt to derive, based on a simple model of such kind of cross-talk between a pair of channels (see Cross-talk model in Methods for details), an analytic relation of the strength of the cross-talk to the correlation between the raw signals of the two channels, and also to the HSE index for these channels. This allows us to further relate the raw signal correlation to the HSE index, which can be directly compared to the relation between these measures observed in the real data (Figure 3e).

In the model we assume the "ground truth" raw signal, which is not contaminated by cross-talk, denoted as x_1 and x_2 for channel 1 and 2, respectively. For simplicity, we assume that they are independent Gaussian white noise time series with the mean 0 and the same variance σ^2. We model the cross-talk as a linear mixing of these two signals (Figure 4a) such that the signals s_1 and s_2 measured on channel 1 and 2, respectively, are obtained as:

$$\begin{aligned} s_1 &= x_1 + \alpha x_2 \\ s_2 &= x_2 + \alpha x_1, \end{aligned}$$

where α is a parameter representing the strength of the crosstalk: s_1 and s_2 are identical when $\alpha = 1$, and they are independent when $\alpha = 0$. The Pearson correlation coefficient c_{12} for the signals s_1 and s_2 is derived as (see Cross-talk model in Methods for derivation):

$$c_{12} = \frac{2\alpha}{1+\alpha^2} \tag{1}$$

Figure 4b shows the correlation coefficient c_{12} plotted against the cross-talk strength α. The correlation c_{12} increases as the cross-talk strength α is increased. The rate of increase is highest at $\alpha = 0$ with a slope of 2, and gradually diminishes with increased α, to reach a slope of 0 at $\alpha = 1$. Thus, the correlation c_{12} is a monotonically increasing convex function of the cross-talk strength α.

As for derivation of the HSE index, which is defined in terms of the number of synchronous spikes across neurons, we need to introduce spikes to the signals. Here we model spikes in channel 1 by adding a value A_1, representing the spike amplitude, to x_1 at various, random time points. We parameterize A_1 as $A = \sigma r_1^{\mathrm{SN}}$, where r_1^{SN} is the signal-to-noise ratio of the spike waveform. The spikes introduced in the ground truth signal x_1 are transferred to

the measured signals s_1 and s_2 via the cross-talk. To count those transferred spikes, we extract spikes from s_1 by thresholding it at $m\sigma_{s_1}$, where $\sigma_{s_1} = \sqrt{1+\alpha^2}\sigma$ is the standard deviation of s_1 and m is a multiplier determining the threshold in relation to the standard deviation. Assuming that N_1 spikes were introduced to x_1, we can derive the expected number n_{11} of the spikes transferred from x_1 and detected in s_1 as $n_{11} = p_{11}(m, r_1^{\mathrm{SN}}, \alpha)N_1$, where p_{11} is a function representing the probability that a spike transferred from the ground truth signal x_1 is detected in the measured signal s_1 (see Cross-talk model in Methods for derivation). In a similar manner, the probability p_{21} that a spike originally in x_1 is detected in s_2, and the probabilities p_{12} and p_{22} that N_2 spikes in the other ground truth signal x_2 are detected in the measured signals s_1 and s_2, respectively, can also be derived (see Cross-talk model in Methods for details). With these probability values, the expected numbers n_1 and n_2 of spikes detected in the measured signals s_1 and s_2, respectively, are represented as:

$$\begin{aligned} n_1 &= p_{11}N_1 + p_{12}N_2 \\ n_2 &= p_{21}N_1 + p_{22}N_2, \end{aligned}$$

given the numbers N_1 and N_2 of spikes in the ground truth signals x_1 and x_2, respectively.

Note that the terms $p_{12}N_2$ and $p_{21}N_1$ represent the number of spikes transferred from the other channel, and hence these spikes are detected in the both of the measured signals. Thus, the sum of these terms: $n_{1,2} = p_{12}N_2 + p_{21}N_1$ represents the number of synchrofacts in this pair of measured signals. Using this, the HSE index $I_{1,2}$ (see Measure of spike synchrony in Methods for definition) between the measured signals s_1 and s_2 can be obtained as a function of N_1, N_2, and p_{ij}s (see Cross-talk model in Methods for the formula), which takes a value between 0 and 1 depending on the parameters.

Figure 4c (left) shows the HSE index $I_{1,2}$ plotted as a function of the cross-talk strength α (through the dependence of p_{ij}s on α). Since this function has three parameters: the signal-to-noise ratios r_1^{SN} and r_2^{SN}, and the threshold multiplier m, here we set the two signal-to-noise ratios identical, i.e., $r_1^{\mathrm{SN}} = r_2^{\mathrm{SN}} = r^{\mathrm{SN}}$, and vary r^{SN} from 5 to 15 in steps of 1, while keeping the threshold multiplier at $m = 5$. The curves in different shades of gray in Figure 4c (left) represent the HSE index for different values of r^{SN}. For all values of r^{SN}, the HSE index $I_{1,2}$ is 0 at $\alpha = 0$ and reaches 1 at $\alpha = 1$. For smaller r^{SN} values (light gray curves), $I_{1,2}$ starts to rise at around $\alpha = 0.25$ and shows a concave curve. This behavior indicates that spikes with small amplitudes (i.e., small r^{SN} values) contribute to synchrofacts only when the cross-talk strength is considerably large (i.e., α values well above 0.25). For larger r^{SN} values (dark gray curves), $I_{1,2}$ starts to rise earlier at smaller α and soon saturates at 1, showing a sigmoid curve. This means that spikes with large amplitudes contribute to synchrofacts even when the cross-talk strength is weak or medium. Furthermore, when the cross-talk is even stronger, all the spikes cause synchrofacts.

Since α can be expressed in terms of c_{12} by solving equation (1), the HSE index $I_{1,2}$ can be directly related to the raw signal correlation coefficient c_{12}. Figure 4c (right) shows the HSE index $I_{1,2}$ as a function of the raw signal correlation coefficient c_{12}. Here again, the threshold multiplier m is fixed to 5 and the signal-to-noise ratio $r^{\mathrm{SN}}(= r_1^{\mathrm{SN}} = r_2^{\mathrm{SN}})$ of spike waveform is varied from 5 to 15 in steps of 1. Owing to the convex dependence of c_{12} on α, the features of the relations between $I_{1,2}$ and α described above are reproduced here with a systematic compression of the plotted curves towards higher c_{12} values. As a result, $I_{1,2}$ starts to rise at around $c_{12} = 0.4$ even for the largest r^{SN} value of 15. This means that, for physiologically plausible values of r^{SN}, channel pairs with a correlation less than 0.4 would hardly exhibit synchrofacts.

So far we have grouped spikes detected in the measured signal of one channel into a single class and did not discriminate spikes that originate from different neurons (in different ground truth signals). In analyses of real spike train data, however, researchers are often interested in treating spikes from different neurons separately and examining properties of the spiking activity of a single individual neuron, i.e., single unit activity (SUA). SUA spikes are sorted out from a spike train obtained from a single channel and (potentially) containing spikes from

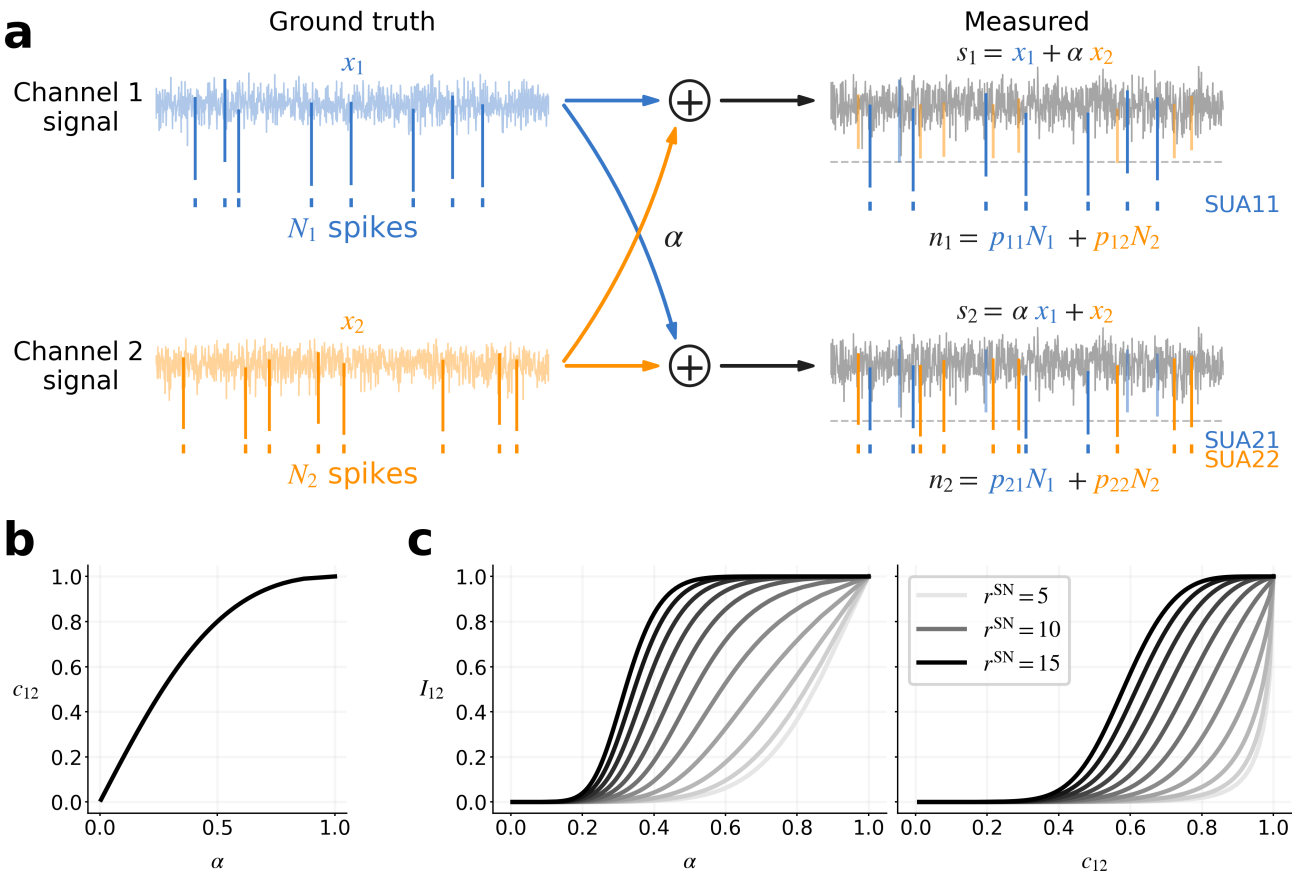

Figure 4: Cross-talk model of synchrofacts. (a) Illustration of the setup for derivation of the HSE index. Ground truth signals for channels 1 and 2 are mixed, representing the cross-talk between the channels, to yield the signals measured in the two channels. Spikes (vertical lines) are introduced to the ground truth signals, and they "bleed" into the measured signal of the other channel via the cross-talk. Spikes in each channel are extracted by thresholding the corresponding measured signal. (b) The correlation c_{12} between the channels plotted against the cross-talk strength α. (c) Left: the HSE index $I_{1,2}$ of the channels plotted against the cross-talk strength α. The threshold multiplier m is set to 5, and the curves for a range of $r^{\mathrm{SN}} (= r_1^{\mathrm{SN}} = r_2^{\mathrm{SN}})$ values are plotted in different shades of gray. For the color convention, refer to the legend in the right panel. Right: the HSE index $I_{1,2}$ of the channels plotted against the correlation c_{12} between the channels. Again the threshold multiplier m is set to 5, and the curves for a range of r^{SN} values are plotted in different shades of gray, as indicated in the legend.

multiple neurons, termed multi-unit activity (MUA), based on the waveforms of individual spikes. In our analyses of experimental spike trains and the cross-talk model, the HSE index has been considered for pairs of channels and computed based on the spike counts of the MUAs of the two channels. We can instead consider and compute the HSE index between individual SUAs in a pair of channels in the same manner as for the MUAs.

Let us examine how the HSE index for SUA pairs differs from what we have considered so far, for the case of the example shown in Figure 4a (right). In this case, only one SUA (blue spikes) would be detected in channel 1, while in channel 2 two SUAs (blue spikes and orange spikes) could be detected, if the waveforms of these two classes of spikes differ distinctly enough for successful spike sorting. Note that although the blue spikes in channel 1 are - although they have different heights - from the same unit, but ride on different background levels. Let us assume that this is actually the case. Then we can consider HSE indices between the following three SUAs: 1) blue spikes in channel 1, named here SUA11, 2) blue spikes in channel 2, named SUA21, and 3) orange spikes in channel 2, named SUA22. Note that there are no synchronous spikes between SUA21 and SUA22, since they are detected in the same channel. Hence, here we need to consider only the HSE indices for SUA11-SUA21 pair and SUA11-SUA22 pair.

For the SUA11-SUA21 pair, the spikes of both SUAs are originally the spikes in the ground truth signal of channel 1, and hence all the spikes of SUA21 (i.e., the spikes transferred from x_1 to s_2) are also found in SUA11 at the same respective spike times, yielding synchrofacts. Thus, the number of these synchrofacts between SUA11 and SUA21 equals the number of SUA21 spikes (and this number is smaller than the number of SUA11 spikes because $p_{12} < p_{11}$ for any $\alpha > 0$), meaning that the HSE index for this SUA pair is 1. Note that this is generally the case for any pair of SUAs that originate from spikes in a single ground truth signal but are detected in different channels due to cross-talk. On the other hand, the HSE index for the SUA11-SUA22 pair should be as small as expected from chance coincidences (assuming no functional correlations between these SUAs), since these SUAs represent independent neurons which are originally recorded in ground truth signals of different channels. Such a small HSE index value is generally the case for any pair of SUAs that originate from spikes in different ground truth signals.

To summarize, the HSE index between SUAs can only take a value of either 1 or a smaller number expected from chance coincidences. This applies to any pair of SUAs as long as spike trains are perfectly sorted into SUAs in all channels. Thus, any intermediate values of HSE index between these two can only exhibited when the index is computed for a pair of MUA spike trains, otherwise such HSE values would indicate that the spike sorting is not perfect and some SUAs include spikes from other SUAs which bleed from other channels due to the cross-talk.

Channel removal for synchrofact mitigation

After we have derived a model describing the cross-talk between two channels, we now consider how we utilize the knowledge from the model to remove the artifacts from our data set. Let us first consider the case where spikes are not sorted into single units, and hence all threshold crossings in a channel are treated as one multi-unit activity (MUA). In this case, the model shows that a high raw signal correlation coefficient indicates a channel pair with a lot of synchrofacts, depending on the signal-to-noise ratios of the spikes in the channels. Thus, one solution to remove synchrofacts in this case would be to discard the MUAs on channels with a strong correlation to any of other channels, and to use only the MUAs on the remaining channels for further analyses. For such screening of channels, we identify for each channel the highest coefficient of correlations with other channels, denoted as C_i for channel i and defined as follows:

$$C_i = \max_{j \neq i}(c_{i,j}) \tag{2}$$

Here, $c_{i,j}$ denotes the correlation coefficient between the raw signals of channel i and j. Consequently, C_i is their maximum. We then choose a threshold value on C_i, such that all channels with a C_i value above this threshold are discarded. Since the analytical result from the model (see Cross-talk model explains the emergence of synchrofacts

in Results) shows that the HSE index grows rapidly as the correlation coefficient increases beyond 0.4, we set the threshold on C_i for our channel screening at 0.4.

To see how the highest correlation coefficient C_i is related to occurrences of HSEs on channel i, we introduce a new measure evaluating each channel with regard to its participation in HSEs with all the other channels. We term this as the global HSE index I_i for channel i, defined as the ratio of the number of HSEs including channel i to the number of all spikes on channel i (see Measure of spike synchrony in Methods for the formula). According to this, the HSE index $I_{i,j}$ that we have introduced before for a pair of channels i and j is now referred to as pairwise HSE index. Figure 5a (left) shows the global HSE indices I_i for all the channels plotted against their respective highest correlation coefficients C_i. As expected from the model, the channels with high correlations in their raw signals are indeed also the channels with high global HSE indices, while the channels with correlations below 0.4 show rather small global HSE indices.

As one approach to remove synchrofacts from the data, one can now discard all channels that have a C_i higher than 0.4. For the present data sets this excludes a lot of channels from the analysis. For example, in the case of macaque Y, over half of the channels are excluded (Figure 5b). After discarding MUAs on those channels, the complexity distribution matches what would be expected from chance coincidences (Figure 5c, middle), indicating that synchrofact HSEs are successfully removed (together with all the spikes on the excluded channels) while keeping chance HSEs on the remaining channels intact.

The channel screening method described above excludes quite a number of channels. Among those, there are a considerable number of channels showing a low global HSE index comparable to those of the channels kept for analyses (Figure 5a, middle). According to the model, these would be the channels with spikes of such small amplitudes that they do not cross the threshold on the other channels (that they bleed into via crosstalk), and hence not causing synchrofacts, and not receiving spikes from other channels either. If this is the case, these channels should contain only the spikes recorded at their respective electrodes, and hence they do not need to be excluded from analyses. This leads to an idea of setting a threshold for channel screening not on the highest correlation coefficient C_i, but on the global HSE index I_i. Therefore we devise a second method to exclude channels as follows: 1) set a threshold for C_i at 0.4; 2) take the highest of the I_i values for all the channels with C_i below this threshold; 3) exclude all channels with an I_i higher than the value in (2). This excludes considerably less channels than the previous method (Figure 5b), but is similar in results with regard to the complexity distribution (Figure 5c). Thus, regardless of which method we choose, if we exclude the right channels, we can avoid most of the synchrofacts. We cannot conclusively proof that the remaining channels do not contain any artifacts anymore, but the data set improves noticeably.

Spike sorting does not ensure synchrofact removal

The results presented until now are based on events that are obtained by setting a threshold in the raw signal and extracting all spike-like deflections of the signal that cross this threshold. Commonly, the complex process of spike sorting is applied to assign the action potentials recorded on one electrode to putative neurons, so-called units. Units may contain the activity of a single neuron or an ensemble of activity of multiple neurons, referred to as single unit activity (SUA) or multi unit activity (MUA), respectively. While the former is used to refer to clearly separated units (i.e., the waveforms assigned to that unit have a high consistency) representing putative single neurons, the latter is often used as a container of all waveforms that have spike-like shapes, which could not be clearly attributed to a single neuron.

The optimal way of achieving this sorting is hindered by the lack of a ground truth and is still an active field of research (see e.g., Buccino et al. (2022)). In the times of single electrode recordings, it was common to sort the waveforms semi-manually, which usually involved the choice of multiple parameters and thresholds. With the increasing number of electrodes recorded simultaneously, this semi-manual process became increasingly time-

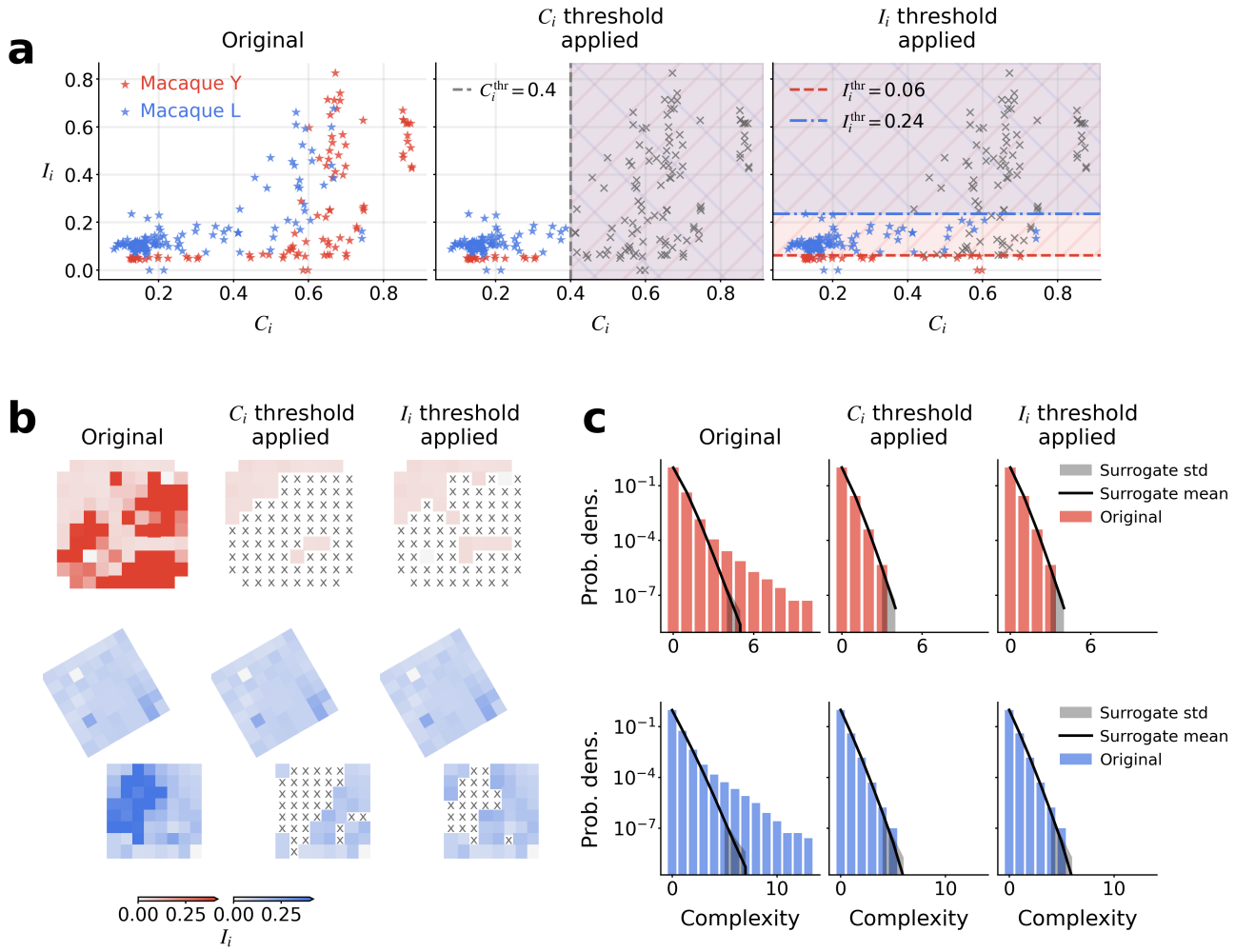

Figure 5: Synchrofact removal based on channel screening. (a) The highest correlation coefficient for channel i (x-axis) vs. the global HSE index I_i for channel i (y-axis). (Left) C_i vs. I_i calculated using all channels. (Middle) Recalculated using only channels with a C_i lower than 0.4. (Right) Recalculated using only channels with an I_i lower than 0.4. (b) Channels excluded by the proposed methods, shown on the electrode grid of the arrays. Crosses indicate the excluded channels. (c) Complexity distribution for the channels remaining after the two channel screening methods (middle and right), compared to the original (left, calculated as in Section Synchronous spike events are ubiquitous in multi-electrode systems).

consuming, giving rise to the development of fully automatic sorters. No matter whether the sorting is semi-manual or automatic, as a side-effect of this sorting procedure, threshold crossings with waveforms that do not resemble action potentials are rejected. In consequence one may assume that spike sorting serves as a valid tool of artifact rejection.

In this section, we investigate whether this is the case using semi-manually sorted data of macaque Y (see Spike Sorting in Methods for the spike sorting procedure). In this example spike extraction thresholds have been set manually for each channel prior to the recording session. Here, the experimenter is faced with the trade-off of setting a threshold beyond the noise floor, but not too far off, such that putative spikes may be not missed. Notably, this differs from the situation described in the model (see Cross-talk model explains the emergence of synchrofacts in Results), where spikes on both channels are extracted with a similar threshold (defined by a multiplier m and the standard deviation). In our example data set, the online extracted waveforms were then sorted with the help of the Plexon Offline Sorter (Plexon Inc, Dallas, Texas, USA). This involves an invalidation of cross-channel artifacts (e.g., chewing artifacts), for which all waveforms that occurred simultaneously on a defined percentage of channels (70%) were marked as "invalidated waveforms". Besides this cross-channel artifact rejection, it is important to notice, that spike sorting was done independently per channel. Therefore, temporal correlation of spikes between channels such as in synchrofacts or similarity of waveforms between channels cannot be noticed during the process. While common noise artifacts (an extreme example is shown in Supplementary Figure S4) will likely be captured by the cross-channel artifact rejection, pairwise or group-wise correlations that are expected in the scenario of cross-talk might go unnoticed.

To further ensure the quality of the spike trains even after spike sorting, typically a number of quality metrics are used to filter the units. Here we only use SUAs, require the waveform signal-to-noise (SNR) per unit to be larger than 2.5 and reject units with a average firing rate $< 1\,\mathrm{Hz}$.

In the following we perform the same analysis as for the thresholded data, but now on spike-sorted pairs of single units and compute the pairwise HSE index $I_{i,j}$ as before (see Measure of spike synchrony in Methods). The indices i and j here denote different SUAs and not channels. Figure 6a shows the pairwise HSE index calculated for SUA pairs plotted against the raw signal correlation coefficient for the channels that the respective SUAs belong to. Since we have less SUAs than channels there are not so many pairs available. Similar to the results from channel pairs (cmp. Figure 3e, left), the pairwise HSE index of SUA pairs $I_{i,j}$ increases with increasing raw signal correlation coefficient $c_{i,j}$. The shape of the graph for the HSE index is as for the channel data, with a sharp increase after $c_{i,j} > 0.4$ and take values between 0 and 1.

We learned from the model (see Cross-talk model explains the emergence of synchrofacts in Results) that well sorted single units would lead to an HSE index of either 1 or a small value expected from chance coincidences. Thus, the obtained result indicates that a considerable part of the SUAs showing intermediate values between 0 and 1 and include spikes that bleed in from other channels via cross-talk, which are missed to be sorted out in the process of spike sorting.

SUAs contaminated by bleeding spikes should be removed from the analyses, since they do not faithfully represent the activity of a single neuron and hence would hamper correct interpretation of a respective analysis result. In the same spirit as for the channel screening described in the previous section (see Channel removal for synchrofact mitigation in Results), we can consider an additional screening on the SUAs that is based on the global HSE index for a SUA i and the highest raw signal correlation coefficient C_i of the channel of that SUA. The global HSE index for a SUA is calculated in the same manner as for a channel (equation (2)), i.e., now as the ratio of the number of SUA i spikes participating in HSEs (with any other SUA j) to the total number of the spikes of SUA i. Figure 6b shows the global HSE index I_i for SUAs plotted against C_i. One can screen SUAs based on this plot, either by setting a threshold on the raw signal correlation coefficient, or on the global HSE index, as we described in the previous section for the channel screening. As shown in the complexity distribution (Figure 6c) we see that we

obtain the same result as we got for spiking activities by threshold crossing: Excluding the worst SUAs removes most of the synchrofacts from the data set. In other words the proposed method remains valid for spike sorted data.

Discussion

We have shown, in data sets of two different laboratories, that a particular kind of artifact occurs in massively parallel electrophysiological recordings. These artifacts become visible as synchronous spike-like events if the data are analyzed on the time scale of their sampling rate. They exhibit spike-like synchrony across neurons (complexities) of up to 10 or more counts, which seem not to be of neuronal origin. These artifacts of spike-like events affect correlation analyses on the millisecond time scale and may lead to false correlations. Our analysis of the relation between the HSE index ($I_{i,j}$), i.e., the occurrence frequency of the highly precise synchronous events and the raw signal correlation coefficient ($c_{i,j}$), i.e., the correlation of the band pass filtered raw signals, measured for pairs of channels i and j, revealed a typical behavior: up to a value of about $c_{i,j} = 0.4$, the HSE index is low, but then rapidly increases to high values. A model of cross-talk causing spikes to bleed from channels into others explains the findings very well. To remove the artifacts we suggest to set a threshold on the maximum raw signal correlation C_i of the ith channel and to exclude all channels with a higher C_i than 0.4 from the data. Interestingly, spike sorting of HSE channels does not necessarily remove the artifacts, but requires subsequent filtering to remove the artifacts. Before taking the approach to remove the artifacts after the recordings, we of course tried to identify the physical sources of the artifacts in the setup, particularly in the setup for macaque Y. There we noticed that short-living electrical blips, e.g. by switching on a light, found entry into the recording signals of multiple channels. It seemed that, to avoid those, large constructions were required in the building or the recording room, e.g. an electrically shielded room. However, these artifacts disappeared with the usage of improved headstages.

We found more artifacts in macaque L data than in macaque Y data. Besides the fact that for the macaque L data we intentionally chose two arrays (out of 16) which particularly showed potential cross-talk artifacts (see Macaque L in Methods), a different type of the headstage was used, which we suspect to be a potential source for synchrofacts. The headstage type was 'Cereplex M' (Blackrock) in macaque L and 'Cereplex E' (Blackrock; a digital headstage, i.e., digital signals from the headstage on) in macaque Y. The former consisted of a lot of freely hanging flat cables, whereas the latter is within a compact box.In a former project we also analyzed additional data sets from an older recording setup from Blackrock (see data sets published in Brochier et al. (2018) and Riehle et al. (2013)), where the headstage was 'Samtec' (Blackrock) for one monkey and the 'Patientcable' (Blackrock) for the other. There the complexities were even larger than in macaque L. To perform the spike synchrony analysis on these data sets in Torre et al. (2016) we removed all spikes that were part of HSEs with complexities ≥ 2. (This analysis contained data of two monkeys, for one of which we did not have the raw signal required for the artifact removal approach introduced here.) This was a rather rigorous step, and led to an underestimation of the excess synchrony in the data (see Figure S1). While the study has already revealed a particular organization of synchronous spike patterns, which is consistent with LFP wave propagation patterns (Rubino et al., 2006; Denker et al., 2018b), re-examination of the same data with our proposed synchrofact removal method might lead to stronger and clearer results.

The online spike sorter in the Blackrock recording system has a built-in artifact removal function, which detects synchronous events of high complexity and removes them online. However, this procedure requires to set a sensible threshold of synchronous events, which is not known beforehand, and if set too low, artifacts may remain undetected. Furthermore, other artifacts, which became apparent as 'holes' in the data stream, are caused by the usage of the online sorter that requires buffering of the data, which can be very memory-intensive. In any case, online sorting of a large number of channels is hardly solidly doable in such a setup. Switching to offline sorting can avoid these problems.

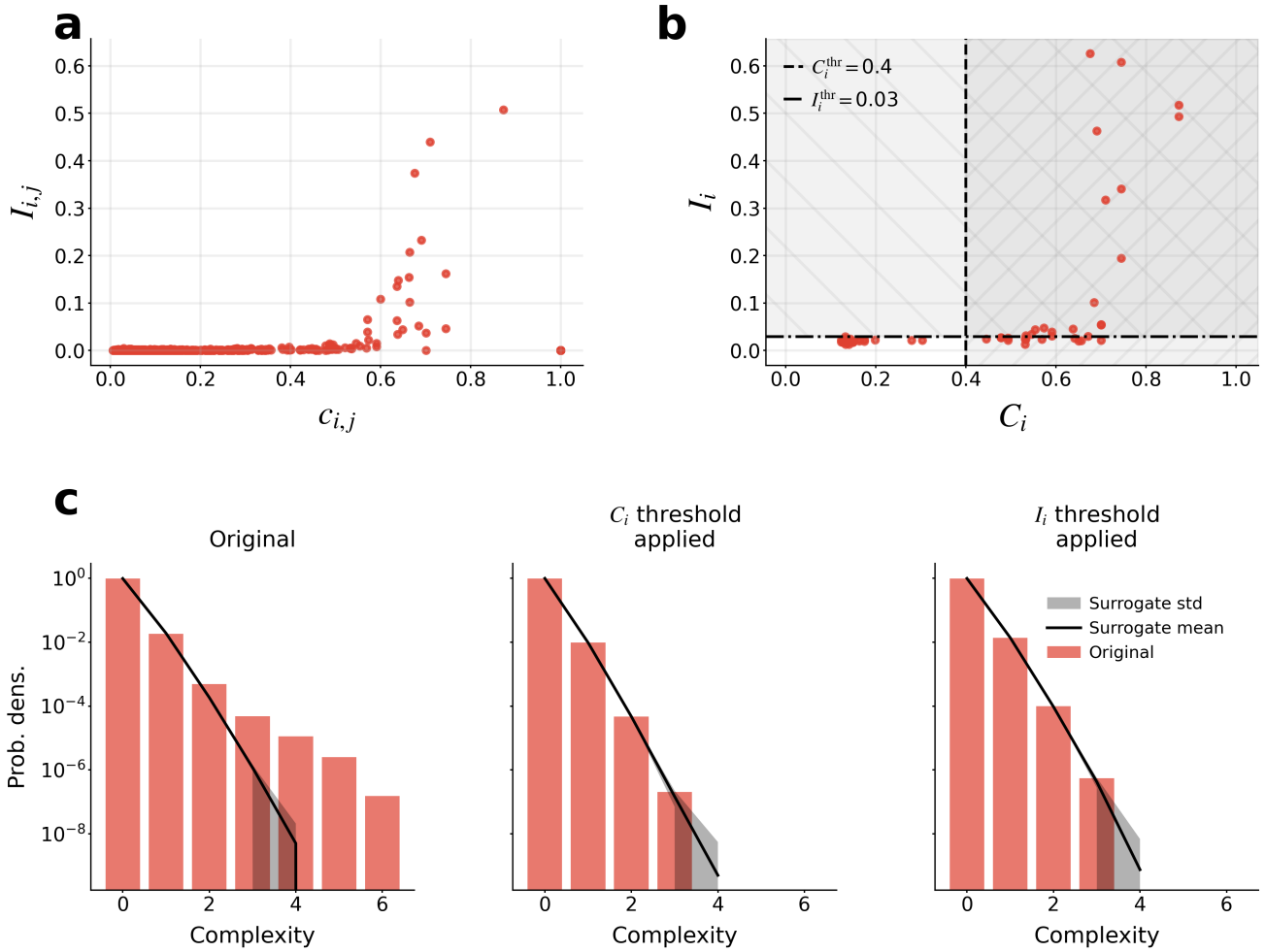

Figure 6: Detection and removal of synchrofacts in spike sorted data from macaque Y. (a) Pairwise HSE index $I_{i,j}$ for SUA pairs vs. raw signal correlation $c_{i,j}$ of the respective channels. Note that a pair of SUAs on an identical channel always yields $(c_{i,j}, I_{i,j}) = (1, 0)$. (b) Global HSE index I_i of SUA i vs. the highest raw signal correlation coefficient C_i of the corresponding channel. The vertical and horizontal lines indicate the threshold for C_i and I_i, respectively, used for removal of SUAs with the proposed method. (c) Complexity distribution computed from the spike sorted data, (left) the original data, (middle) data after SUA removal with the C_i thresholding method, (right) data after SUA removal based on the I_i thresholding method.

All these aspects have been taken into account in the setup for macaque Y: no online spike sorting, a greatly improved headstage, no threshold setting for artifacts, and recording of the broad band raw signal. However, we still have some cross-talk artifacts as identified here. Since we and the experimenters could not track down the origin of this cross-talk, we decided to remove the artifacts using the algorithms shown here.

One may wonder if recordings using other electrodes, such as high-density Neuropixel electrodes, may be less affected by such artifacts. The Neuropixel electrodes record individual neurons on more than a single recording site, since electrodes are much closer (40 μm) to each other than on the Utah array (400 um), which enables spike sorting that takes into consideration more than one signal per neuron, e.g. by using the Kilosort sorter (Steinmetz et al., 2021; Pachitariu et al., 2023). In Jain et al. (2022), we introduced an adaptive analysis pipeline for automated denoising and evaluation of high-density electrophysiological recordings. Here, similar artifacts appeared as hyper-synchronous spike clusters that were removed on the basis of comparison to the spike dithered complexity distribution. Visual control and manual intervention enabled to remove the artifacts.

We have suggested two approaches to remove the synchrofacts: applying a threshold on the channel-wise maximum correlation C_i of the raw signals (≤ 0.4, vertical threshold), or a threshold on the global HSE index I_i (horizontal threshold, set based on I_i of channels with low C_i). Applying the vertical threshold excludes slightly more channels than the horizontal method, but the ones that are kept are more in agreement with what is expected by chance and are thus more reliable than the remaining channels after applying the horizontal threshold. On the one hand the first approach excludes spike trains that arguably do not contain many synchrofacts, on the other hand channels with high correlation coefficients are definitely flawed. Which approach to take depends on the analysis to be performed on the resulting data. Spike correlation analysis requires completely synchrofact-free data, but an analysis based on firing rates may be unimpaired by HSEs (however, see Figure 7a).

In a previous study some of us (Chen et al., 2022) defined a 'synchrofact participation' (SP) ratio as the number of synchronous spike events above chance, derived by a bootstrap method on the complexity distribution. The channels with highest SP were removed iteratively. The authors discussed that while the electrode removal process eliminates a large portion of the spurious correlations, it does not reject artifacts that occur sporadically or at low rates on a given electrode.

An obvious idea is that false 'spikes' are filtered out by spike sorting. However, following our model, the cross-talk copies spikes into other channels without distorting the waveform, and therefore the copied spikes cannot be distinguished from real spikes, besides the smaller amplitude. In fact, in a former study (not shown here) we tried to discriminate between real spikes and artifact spikes by cross-correlating spike shapes, but we were not able to separate false from real spikes. Here we found that also in spike sorted data synchrofacts are present, demonstrating that spike sorting does not completely remove artifact spikes. However, spike sorted data show less artifacts than unsorted data, thereby proving that spike sorting reduces the problem.

Synchrofacts that remain unnoticed in the data can affect the results and interpretation of various analyses. Here we demonstrate the impact of synchrofacts on two types of analyses. One question is, if synchrofacts influence firing rates in a relevant way. For testing this we simulate spike trains of motor cortex neurons with a hand movement direction preference (Georgopoulos et al., 1982). Further we make the Ansatz that the firing rate of a neuron is modulated in a sinusoidal manner as a function of the direction of the hand movement, with the highest firing rate occurring at the preferred hand movement direction. Here, we consider a pair of neurons with different preferred directions, mean firing rates, and rate-modulation depths. We assume that these neurons are recorded in two separate channels, which are cross-talking with a cross-talk strength α. We regard one channel as the source of the artifact spikes, which provides spikes from its signal to the other channel, referred to as the target channel. The neurons in the source and target channel are referred to as the source neuron and the target neuron, respectively.

With this setup, we examine how the tuning curve estimated from the spike train measured in the target channel is modulated when spikes are merged between the two channels due to the cross-talk (Figure 7a). We consider various

levels of cross-talk strength α and their impact on the tuning curve estimated from the spikes measured in the target channel (gray curves in Figure 7a). The three examples in Figure 7a illustrate cases with different combinations of mean firing rates, modulation depths, and preferred directions (PDs). In Figure 7a (left) the target neuron has a PD of 180 deg (blue curve) and the source neuron has a PD of 90 deg (orange curve), and both have the same mean rate and the same modulation depth. With increasing cross-talk strength, the mean response and the modulation depth estimated from the measured spike train in the target channel gets larger, and in particular, the peak of the estimated tuning curve shifts closer to the source PD, because the activity introduced from the source channel by the cross-talk increases with the increased cross-talk strength. Figure 7a (center) shows a similar example, where the target neuron has a lower mean rate and smaller modulation depth than the source neuron, while the PDs of both neurons are unchanged. As in the first case, the estimated tuning curve changes with increasing α, but here it reaches a much higher similarity to the source tuning due to the mean rate of the source neuron being higher than that of target neuron. In Figure 7a (right), the two PDs are opposite, the target at 180 deg as before, the source at 0 deg. Due to the high mean firing rate and large modulation depth of the source neuron, the estimated PD becomes more and more similar to the source PD with increasing cross-talk strength, switching the PD by 180 deg, and its firing rates become much higher than the original target neuron. We conclude from these examples that the preferred direction of the tuning can become considerably altered by the cross-talk, as can the tuning response. High firing rate of a neuron do not mean that it is not impacted by cross-talk. Thus, cross-talk can have strong effects on an as simple analysis as tuning curve estimation.

Another example of the impact of synchronfacts is on the analyses for excess spike synchrony using the Unitary Event analysis as explained in Unitary Event analysis in Methods. The Unitary Event analysis (Grün et al., 2002a,b; Grün & Rotter, 2010) enables to derive excess spike synchrony from a simultaneously recorded pair of spike trains by computing the empirical and the expected number of synchronous spike events. Here we consider a pair of independent Poisson spike trains (10 Hz firing rate, 5 sec duration) as the ground truth spike signals of a pair of channels, and examine how the cross-talk between these channels affects the result of the Unitary Event analysis on the spike trains measured from these channels. According to our model, the empirical number n_{emp} of synchronous spike events is obtained as $n_{1,2}$ derived in Subsection Cross-talk model explains the emergence of synchrofacts, while the expected number n_{exp} is calculated from the firing rates of the measured spike trains. Figure 7b (left) shows the difference between n_{emp} and n_{exp} as a function of raw signal correlation between the two channels, for a range of the ground truth spike amplitude r^{SN}. The stronger the raw signal correlation (due to the stronger cross-talk), the more spikes are copied into the other channel (see Cross-talk model explains the emergence of synchrofacts in Results) and thus more synchrofacts are generated, resulting in the increased difference between the empirical and the expected number of spike synchrony. This effect is stronger the larger spike amplitude r^{SN}. As a consequence, for large raw signal correlation values, the significance of the difference (Figure 7b, right), expressed here as the surprise (see Unitary Event analysis in Methods), rises beyond the 5% significance level, i.e., false positive excess spike synchrony is detected. The larger the spike amplitude r^{SN}, the lower the value of $c_{i,j}$ for which the surprise crosses the significance threshold. This result shows that, if cross-talk goes unnoticed, the data may be wrongly assumed to contain excess spike synchrony. This will also happen when the data are binned at larger bin sizes (e.g. 1 ms or more) than the time scale of the synchrofacts. Removing channels as proposed here to remove artifacts leads to a removal of the false positive results.

The complete removal of the HSEs with complexities > 1 on the 1/30 ms time scale, instead of the proposed channel removal, will cause damage to the data. The lack of chance synchrony can be noticed on a larger time resolution on the order of ms. As a result the surprise will be negative and potentially existing neuronal excess spike synchrony may be masked by this effect (Oberste-Frielinghaus, 2022).

These are just two examples that show the influence of synchrofacts on different analyses, but it is to be expected that other types of analyses are affected similarly and can also produce wrong results in the presence of synchrofacts.

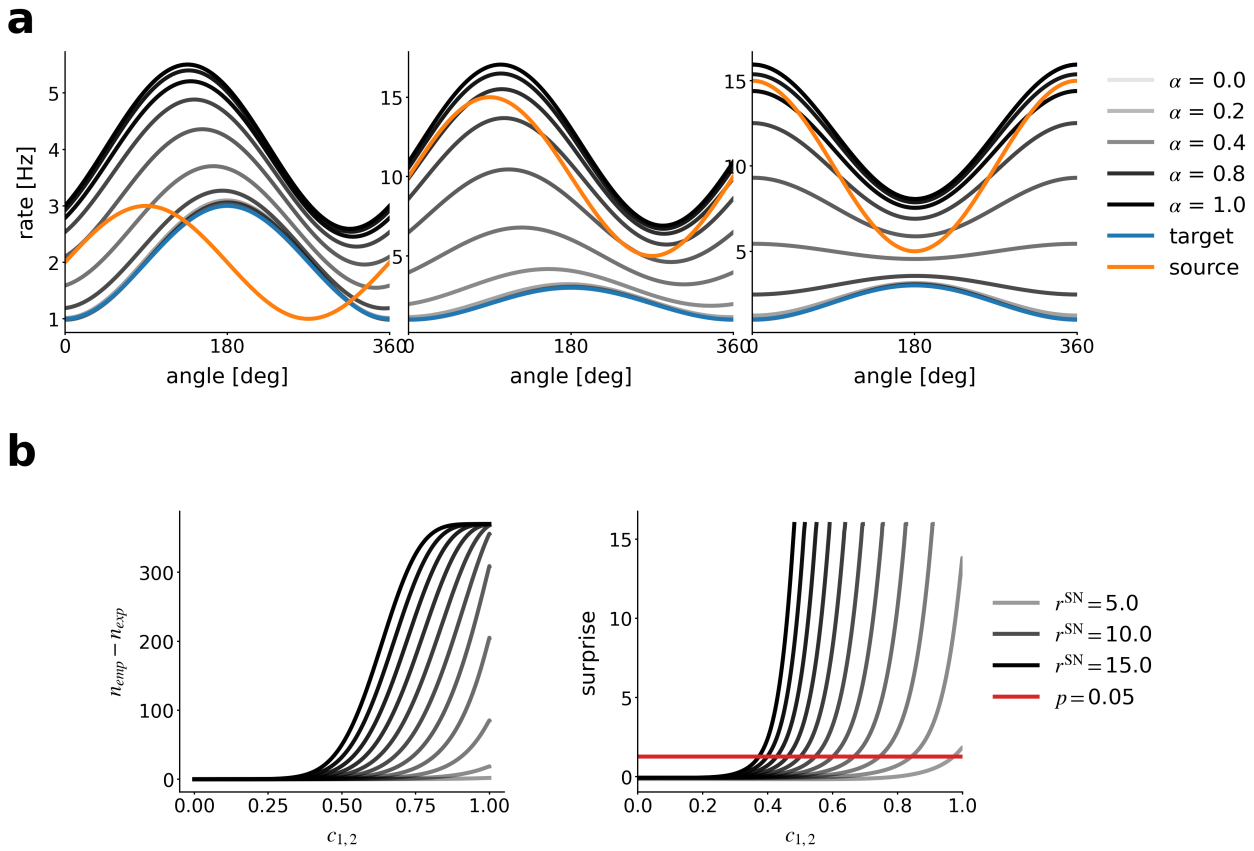

Figure 7: Impact of synchrofacts on data analyses. (a) Impact on neuronal tuning, for three example cases with different combinations of target and source neuron's tuning properties. The tuning curves of the target and source neuron are shown by blue and orange curves, respectively. The tuning curve estimated from the spike trains measured in the target channel is shown in gray, with different shades according to the cross-talk strength α as indicated in the legend to the right. (b) Impact on Unitary Event analysis. Left: excess spike synchrony, measured as the difference between the empirical and expected number of synchronous spike events, as a function of raw signal correlation. Right: surprise of the excess synchrony as a function of raw signal correlation. The surprise value corresponding to the 5% significance level is indicated by the red horizontal line. In both plots, results for different values of spike amplitude r^{SN} are shown in different shades of gray.

For this reason one should make considerable efforts to avoid synchrofacts as much as possible.
In summary, we suggest to test the complexity distribution derived from data on the sampling rate resolution for indications of artifacts by comparison to surrogates. This computation is rather simple, and if synchrofacts are detected, they should be removed. The solution we suggested here requires to have access to the 'raw data', i.e., the original broad band signal at sampling resolution, and assumes cross-talk as the primary origin of the artifacts. This enables us to relate the pairwise correlation of spike-like events to the broadband signal correlation, and remove the channels whose signals bleed into other channels. If that procedure does not remove all artifacts (according to the complexity distribution), different artifacts may be present and should also be removed to avoid false results. In the data sets we examined here, cross-talk was supposedly the primary origin of synchrofacs, and our proposed method effectively removed the synchrofacts by excluding the channels showing strong signatures of the cross-talk. Since synchrofact seems ubiquitous among various setups for multielectrode array recording and its presence affects various types of analysis, detection and removal of synchrofact is crucial for avoiding false results and ensuring sound interpretation of the obtained results.

Methods

RESOURCE AVAILABILITY

Lead contact

Further information and requests for resources should be directed to and will be fulfilled by the lead contact, Jonas Oberste-Frielinghaus (j.oberste-frielinghaus@fz-juelich.de).

Materials availability

This study did not generate new unique reagents.

Data and code availability

The electrophysiology data from macaque L were previously published and are publicly accessible Chen et al. (2022). The electrophysiology data for macaque Y, together with all processed data for this project (threshold crossings, cross-correlation, HSE index etc.) have been deposited in a GIN repository and are publicly available at the time of publication under a Creative Commons Attribution-ShareAlike 4.0 International Public License. The DOI to the repository is listed in the key resources table. All original code has been deposited at the same GIN repository and is publicly available as of the date of publication. The DOI to the repository is listed in the key resources table. Any additional information required to reanalyze the data reported in this paper is available from the lead contact upon request.

EXPERIMENTAL MODEL AND STUDY PARTICIPANT DETAILS

Macaques

We analyzed the resting state data from two (N=2) rhesus macaques (*Macaca mulatta*), recorded in two different experimental laboratories. The data from macaque L was collected at the Netherlands Institute for Neuroscience, and previously published (Chen et al., 2022). The data from macaque Y was collected at the Institut de Neurosciences de la Timone, with the recording apparatus described in de Haan et al. (2018). At the time of the array implantation macaque L (male) was 7 years old and weighed ∼11kg; and macaque Y (female) was 6 years old and weighed ∼7kg. All experimental and surgical procedures for macaque L complied with the NIH Guide for

Care and Use of Laboratory Animals, and were approved by the institutional animal care and use committee of the Royal Netherlands Academy of Arts and Sciences (approval number AVD-8010020171046). All experimental and surgical procedures for macaque Y were approved by the local ethical committee (C2EA 71; authorization Apafis#13894-2018030217116218v4) and conformed to the European and French government regulations.

METHOD DETAILS

Data collection

Both macaques were recorded using setups based on the Blackrock Microsystems ecosystem.

Macaque L See Chen et al. (2022) for an in-depth description of this data set. Briefly, electrophysiological signals originating from the V1 and V4 regions were recorded using a configuration of 1024 channels distributed across 16 Utah Arrays, each comprising 8x8 electrodes. Sampling was performed at a rate of 30 kHz. The signal pathway commenced with the passive conduction of neuronal signals from the 1024-channel pedestal to an Electronic Interface Board (EIB). This EIB was equipped with 32 36-channel Omnetics connectors, facilitating the interface with eight 128-channel CerePlex M headstages. Notably, the CerePlex M headstages applied a 0.3–7500 Hz analog filter at unity gain, refraining from signal amplification. Analog-to-digital conversion (ADC) was conducted by the CerePlex M, employing a 16-bit resolution with a sensitivity of 250 nV/bit. The digitized signal was subsequently routed to a 128-channel Digital Hub, with each Digital Hub processing data originating from one CerePlex M, which in turn was linked to two electrode arrays. The Digital Hub undertook the conversion of the digital signal into an optic-digital format. This transformed signal was then transmitted via an optic-fiber cable to a 128-channel Neural Signal Processor (NSP) for subsequent processing and storage. Each Digital Hub supplied the signal to a single NSP. In total, eight NSPs were employed, with each NSP managing data derived from two electrode arrays. In the present study, we focused on a single data stream (NSP1) from one session, which included one array in V1 and one array in V4. These arrays showed many synchrofacts in a previous less exhaustive analysis Chen et al. (2022), including events across both arrays, even though they were separated by the lunate sulcus. Thus, this data stream was particularly useful to demonstrate the non-neural origin of the synchrofacts. Before the analysis we spotted a large artifact event by eye (see Common noise artifact example) which we cut out before the analysis of the data.

Macaque Y Electrophysiological signals originating from V1, V2, DP, and 7A were recorded with four separate 6x6-electrode Utah Arrays. Additionally, M1/PMd was recorded with a 10x10-electrode Utah Array. Sampling was performed at a rate of 30 kHz. In contrast to monkey L, the signal pathway commenced with two 128-channel pedestals (CerePort): One for the four 36-channel arrays and one for the 100-channel array. Each of the pedestals interfaced with a 128-channel CerePlex E headstage. Notably, the CerePlex E headstages applied a 0.3–7500 Hz analog filter at unity gain, refraining from signal amplification. Analog-to-digital conversion (ADC) was conducted by the CerePlex E, employing a 16-bit resolution with a sensitivity of 250 nV/bit. The digitized signal was subsequently routed to a 128-channel Digital Hub, with each Digital Hub processing data originating from one CerePlex E, which in turn was linked to one 100-channel array or four 36-channel arrays. The Digital Hub undertook the conversion of the digital signal into an optic-digital format. This transformed signal was then transmitted via an optic-fiber cable to a 128-channel Neural Signal Processor (NSP) for subsequent processing and storage. Each Digital Hub supplied the signal to a single NSP. In total, two NSPs were employed. In the present study, we focused on the M1/PMd array from one session, to demonstrate that synchrofacts are not limited to visual processing areas.

Signal processing and threshold crossings

All offline signal processing steps (except for spike sorting) and data analysis described below were performed by original custom codes written in the Python programming language and executed in a pipeline defined as a Snakemake workflow (Mölder et al., 2021). The recorded raw signals were band-pass filtered in the frequency range of 250 Hz − 7500 Hz (a second order Butterworth filter, as implemented in the `signal_processing.butter()` function in the Elephant toolbox (Denker et al., 2018a)). According to Quiroga (2007), putative spikes were extracted from the high-pass filtered raw signal of each channel by thresholding it at

$$\text{Threshold} = -5 \cdot \text{median}\left(\frac{|s_i|}{0.6745}\right),$$

where s_i denotes the high-pass filtered raw signal of channel i. The time of threshold crossing of each putative spike was registered as the time of that spike. The resulting spike times per channel were taken as the spike train of the multi-unit activity of that channel.

Spike Sorting

Spike sorting was performed only on the macaque Y data. Details of the sorting procedure are described in Brochier et al. (2018). The essential steps are as follows. The spike waveforms which were extracted and saved during the recording were offline sorted using the Plexon Offline Sorter (version 3.3.3). We started by merging all online extracted waveforms back into one pool per channel and marking them as "unsorted waveforms" in the Plexon Offline Sorter. For the invalidation of cross-channel artifacts (e.g., chewing artifacts), all waveforms that occurred simultaneously on a defined percentage of channels (70%) were then marked as "invalidated waveforms" in the Plexon Offline Sorter. Furthermore, a waveform rejection was performed. Thereby all waveforms of abnormally large amplitude and/or atypical shape on a channel were manually also marked as "invalidated waveforms" in the Plexon Offline Sorter. The actual spike sorting was then performed on the remaining unsorted waveforms (i.e., those not marked as invalidated waveforms) individually for each channel. We used different algorithms to split these waveforms into clusters in a 2- or 3-dimensional principal component (PC) space. The dimensionality of the PC space was chosen according to the best separation. The main algorithms used were K-Means(-Scan) and Valley Seeking (chosen according to the best separation). We used a fixed threshold for outliers (a parameter to be determined in the Plexon Offline Sorter) between 1.8 (K-Means) and 2 (Valley Seeking) to get comparable sorting results. The spikes of the sorted clusters were then controlled using the inter-spike interval (ISI) distributions and the auto- and cross-correlation plots. Clusters with unacceptable outcomes (completely or partly overlapping waveforms), including those with only a few spikes, were left assigned as "unsorted waveforms" in the Plexon Offline Sorter.

Cross-talk model

Electric cross-talk between channels and its influence on the signals are modeled as follows. First, we consider the "ground truth" signals (i.e., not contaminated by cross-talk) $x_1(t_i)$ and $x_2(t_i)$ for channel 1 and 2, respectively, where t_i $(i = 1, 2, 3, ...)$ are discrete sampling timings. For simplicity, we assume that x_1 and x_2 are time series of independent Gaussian white noise with the same mean $E[x_1] = E[x_2] = 0$ and the same variance $\text{Var}(x_1) = \text{Var}(x_2) = \sigma^2$.

Next, we model the cross-talk as a linear mixing of these two signals. Concretely, we define the measured signals

$s_1(t_i)$ and $s_2(t_i)$ for channel 1 and 2, respectively, as:

$$\begin{aligned} s_1 &= x_1 + \alpha x_2 \\ s_2 &= x_2 + \alpha x_1, \end{aligned}$$

where α is a parameter representing the strength of the crosstalk: s_1 and s_2 are identical when $\alpha = 1$, and they are independent when $\alpha = 0$. By this construction, both s_1 and s_2 obey a Gaussian distribution with the mean $E[s_1] = E[s_2] = 0$ and the variance $\mathrm{Var}(s_1) = \mathrm{Var}(s_2) = (1+\alpha^2)\sigma^2$. The Pearson correlation coefficient c_{12} for the signals s_1 and s_2 is derived as:

$$\begin{aligned} c_{12} &= E\left[s_1 s_2\right] / \left(\sqrt{E\left[s_1^2\right]}\sqrt{E\left[s_2^2\right]}\right) \\ &= E\left[\left(x_1+\alpha x_2\right)\left(x_2+\alpha x_1\right)\right] / \left(\sqrt{E\left[\left(x_1+\alpha x_2\right)^2\right]}\sqrt{E\left[\left(x_2+\alpha x_1\right)^2\right]}\right) \\ &= 2\alpha\sigma^2 / \left(\sqrt{\left(1+\alpha^2\right)\sigma^2}\sqrt{\left(1+\alpha^2\right)\sigma^2}\right) \\ &= = 2\alpha / \left(1+\alpha^2\right). \end{aligned}$$

We further introduce spikes to the signals. Here we model spikes in channel 1 by adding a value A_1, representing the spike amplitude, to x_1 at various, random time points. We parameterize A_1 as $A = \sigma r_1^{\mathrm{SN}}$, where r_1^{SN} is the signal-to-noise ratio of the spike waveform, such that SUAs with different spike amplitudes are represented by modifying the value of r_1^{SN}. The spikes introduced in the ground truth signal x_1 are transferred to the measured signals s_1 and s_2 via the cross-talk. To count those transferred spikes, we extract spikes from s_1 by thresholding it at $m\sigma_{s_1}$, where $\sigma_{s_1} = \sqrt{1+\alpha^2}\sigma$ is the standard deviation of s_1 and m is a multiplier determining the threshold in relation to the standard deviation. Assuming that N_1 spikes were introduced to x_1, we can derive the expected number n_{11} of the spikes transferred from x_1 and detected in s_1 ($= x_1 + \sigma r_1^{\mathrm{SN}} + \alpha x_2$ at spike times) as:

$$\begin{aligned} n_{11} &= N_1 \cdot P\left(x_1 + \sigma r_1^{\mathrm{SN}} + \alpha x_2 > m\sigma_{s_1}\right) \\ &= N_1 \cdot P\left(x_1 + \alpha x_2 > \left(\sqrt{1+\alpha^2}m - r_1^{\mathrm{SN}}\right)\sigma\right) \\ &= N_1 \cdot P\left(\mathcal{N}\left(0, \left(1+\alpha^2\right)\sigma^2\right) > \left(\sqrt{1+\alpha^2}m - r_1^{\mathrm{SN}}\right)\sigma\right) \\ &= N_1 \cdot P\left(\mathcal{N}\left(0,1\right) > m - r_1^{\mathrm{SN}}/\sqrt{1+\alpha^2}\right) \\ &= N_1 \cdot \mathrm{erfc}\left(\left(m - r_1^{\mathrm{SN}}/\sqrt{1+\alpha^2}\right)/\sqrt{2}\right)/2, \end{aligned}$$

where $\mathrm{erfc}(\cdot)$ is the complementary error function. [1]

Note that the factor $p_{11} \equiv \mathrm{erfc}\left(\left(m - r_1^{\mathrm{SN}}/\sqrt{1+\alpha^2}\right)/\sqrt{2}\right)/2$ in front of N_1 in the above expression represents the probability that a spike transferred from the ground truth signal x_1 is detected in the measured signal s_1. In a similar manner, the probability p_{21} that a spike originally in x_1 is detected in s_2 is derived as $\mathrm{p}_{21} = \mathrm{erfc}\left(\left(m - \alpha r_1^{\mathrm{SN}}/\sqrt{1+\alpha^2}\right)/\sqrt{2}\right)/2$. Furthermore, assuming N_2 spikes in the other ground truth signal x_2, the probabilities p_{12} and p_{22} that those spikes are detected in the measured signals s_1 and s_2, respectively, are derived as $p_{12} = \mathrm{erfc}\left(\left(m - \alpha r_2^{\mathrm{SN}}/\sqrt{1+\alpha^2}\right)/\sqrt{2}\right)/2$ and $p_{22} = \mathrm{erfc}\left(\left(m - r_2^{\mathrm{SN}}/\sqrt{1+\alpha^2}\right)/\sqrt{2}\right)/2$.

With these probability values, the expected numbers n_1 and n_2 of spikes detected in the measured signals s_1 and

[1] Note that, for simplicity, this formalism does not consider "noise" spikes which arise from the random fluctuations of the background signal that happen to cross the threshold by chance.

s_2, respectively, are represented as:

$$\begin{aligned} n_1 &= p_{11}N_1 + p_{12}N_2 \\ n_2 &= p_{21}N_1 + p_{22}N_2, \end{aligned}$$

given the numbers N_1 and N_2 of spikes in the ground truth signals x_1 and x_2, respectively. Note that the terms $p_{12}N_2$ and $p_{21}N_1$ represent the number of spikes transferred from the other channel, and hence these spikes are detected in the both of the measured signals. Thus, the sum of these terms: $n_{1,2} = p_{12}N_2 + p_{21}N_1$ represents the number of synchrofacts in this pair of measured signals. Using this, the HSE index $I_{1,2}$ between the measured signals s_1 and s_2 (synchrofact index) is expressed as:

$$I_{1,2} = \begin{cases} n_{1,2}/n_1 = (p_{12}N_2 + p_{21}N_1) \,/\, (p_{11}N_1 + p_{12}N_2) & (n_1 \leq n_2) \\ n_{1,2}/n_2 = (p_{12}N_2 + p_{21}N_1) \,/\, (p_{21}N_1 + p_{22}N_2) & (n_1 > n_2) \end{cases},$$

which takes a value between 0 and 1 depending on the parameters.

QUANTIFICATION AND STATISTICAL ANALYSIS

Complexity and estimation of chance levels

To study fine-temporal correlation and also to detect potential synchronous artifacts in parallel spike train data, we first bin the time axis of the spike trains with a predefined bin width (in the present study we use 1, 0.1, and 1/30 ms bins) and compute the complexity of spiking activity at each bin, i.e., the number of units contributing spikes to that bin. Then we make a histogram of the complexity values for all the bins throughout the recording, called complexity distribution. Synchronous spike correlation (or artifactual spike coincidences) of two or more units affects the entries in the complexity distribution for higher complexities (Grün et al., 2008). For easier comparison of the results from different data sets, the histogram is normalized by dividing the counts of all complexities (including the complexity of zero, i.e., the bins with no spikes) by the total number of the bins, such that the sum of the histogram values over all complexities equals to unity.

To elucidate if the complexity distribution obtained from real data indicates excess spike synchrony above a chance level, we compare the empirical distribution to the one from independent data, which we estimate from surrogate data, i.e., modified versions of the original data where the timings of the spikes are intentionally altered. In Stella et al. (2022) the authors compared a number of surrogate methods, and according to that, we employ here the 'time-shift' method (with a 30 ms shift width), by which the spike trains are randomly shifted in time against each other. We generate 200 surrogate spike train data sets, and for each of them we compute the complexity distribution. The mean and standard deviation of the count are calculated for each complexity, and plotted together with the empirical complexity distribution for comparison.

Cross-correlation of high-pass filtered raw signals

The correlation c_{ij} between the raw signals of channel i and j is evaluated by the Pearson correlation coefficient as:

$$c_{i,j} = \frac{\mathrm{Cov}(s_i, s_j)}{\sqrt{\mathrm{Var}(s_i)\mathrm{Var}(s_j)}},$$

where s_i and s_j represent the high-pass filtered raw signals of channel i and j, respectively, obtained as described in Signal processing and threshold crossings, and $\mathrm{Var}(s_i)$ and $\mathrm{Cov}(s_i, s_j)$ represent the variance of s_i and the covariance between s_i and s_j, respectively.

Measure of spike synchrony

Assume that we have n_i spikes in channel i at times t_i^p $(1 \leq p \leq n_i)$. We discretize the time axis in bins of width b, which should be small enough to contain at most one spike in a bin, and obtain a set of bin indices $T_i = \{\tau_i^p | 1 \leq p \leq n_i\}$, which indicates the positions of the time bins where the spikes are observed (in other words, the time of the p-th spike is in the time range $(\tau_i^p b, (\tau_i^p + 1)\, b))$. The number $n_{i,j}$ of spike synchrony events between channels i and j is obtained as $n_{i,j} = |T_i \cap T_j|$. The pairwise HSE index $I_{i,j}$, a measure of the abundance of spike synchrony events between a pair of channels i and j, is defined as

$$I_{i,j} = \frac{n_{i,j}}{\min(n_i, n_j)}.$$

Also, the global HSE index I_i, a measure of the abundance of spike synchrony events between channel i and any other channel, is defined as

$$I_i = \frac{n_{i,\bar{i}}}{n_i},$$

where $n_{i,\bar{i}}$ is defined as $n_{i,\bar{i}} = |T_i \cap \bigcup_{j \neq i} T_j|$, which represents the number of spike synchrony events between channel i and any other channel.

Unitary Event analysis

The Unitary Event analysis (Grün et al., 2002a,b; Grün & Rotter, 2010) is a statistical method which enables to derive excess spike synchrony from a simultaneously recorded pair of spike trains. The method computes the empirical and the expected number of synchronous spike events and evaluates the statistical significance of the difference between the two. Suppose that we have two simultaneously recorded spike trains of duration T. We bin the time with a bin width of b and count spikes of each spike train (if multiple spikes are in a bin, the count is clipped to 1). Then we count the empirical number n_{emp} of spike coincidences by counting the number of filled bins at the same timings in both spike trains. Next, we compute the expected number n_{exp} of spike coincidences in the following steps: 1) estimate the spiking probabilities p_1 and p_2 for the two spike trains, by dividing the total number of spikes in each spike train by the total number of the bins (i.e., T/b). 2) by assuming independence of the spike times of the two spike trains, we estimate the probability of spike coincidence in a bin as $p_1 p_2$. 3) obtain the expected number n_{exp} of spike coincidences by multiplying the coincidence probability by the total number of bins, i.e., $n_{exp} = p_1 p_2 T/b$. If the spike trains obey the Poisson statistics, the spike coincidence count should obey a Poisson distribution of the mean n_{exp}. Hence, the p-value of the empirical coincidence count n_{emp} can be derived (under the null-hypothesis of Poisson spike trains) as $p = \Sigma_{n=n_{emp}}^{\infty} P_{poisson}(n|n_{exp})$. The significance of the p-value is quantified by the joint surprise S defined as $S = \log_{10}(1-p)/p$.

Acknowledgements

We thank Julia Sprenger, Vahid Rostami and Emiliano Torre for previous work on artifacts. We thank Alexa Riehle for manually spike sorting the data of macaque Y. This project has received funding partly from the European Union's Horizon 2020 Framework Programme for Research and Innovation under Specific Grant Agreement No. 945539 (Human Brain Project SGA3), the NRW-network 'iBehave' (grant number: NW21-049) and by the Deutsche Forschungsgemeinschaft (DFG, German Research Foundation) - 368482240/GRK2416 and the DFG Priority Program (SPP 2041 "Computational Connectomics") [S.J.van Albada: AL 2041/1-1].

References

Barban, F., Chiappalone, M., Bonassi, G., Mantini, D., & Semprini, M. (2021). Yet another artefact rejection study: an exploration of cleaning methods for biological and neuromodulatory noise. J. Neural Eng. *18*, 0460c2.

Bell, A. J. & Sejnowski, T. J. (1995). An Information-Maximization Approach to Blind Separation and Blind Deconvolution. Neural Comput. *7*, 1129–1159.

Blot, A. & Barbour, B. (2014). Ultra-rapid axon-axon ephaptic inhibition of cerebellar Purkinje cells by the pinceau. Nat. Neurosci. *17*, 289–295.

Brochier, T., Zehl, L., Hao, Y., Duret, M., Sprenger, J., Denker, M., Grün, S., & Riehle, A. (2018). Massively parallel recordings in macaque motor cortex during an instructed delayed reach-to-grasp task. Sci. Data *5*, 180055.

Buccino, A. P., Garcia, S., & Yger, P. (2022). Spike sorting: New trends and challenges of the era of high-density probes *4*, 022005.

Butts, D. A., Weng, C., Jin, J., Yeh, C.-I., Lesica, N. A., Alonso, J.-M., & Stanley, G. B. (2007). Temporal precision in the neural code and the timescales of natural vision. Nature *449*, 92–95.

Chen, X., Morales-Gregorio, A., Sprenger, J., Kleinjohann, A., Sridhar, S., Van Albada, S. J., Grün, S., & Roelfsema, P. R. (2022). 1024-channel electrophysiological recordings in macaque V1 and V4 during resting state. Sci. Data *9*, 77.

Churchland, M. M., Yu, B. M., Ryu, S. I., Santhanam, G., & Shenoy, K. V. (2006). Neural Variability in Premotor Cortex Provides a Signature of Motor Preparation. J. Neurosci. *26*, 3697–3712.

Dann, B., Michaels, J. A., Schaffelhofer, S., & Scherberger, H. (2016). Uniting functional network topology and oscillations in the fronto-parietal single unit network of behaving primates. eLife *5*, e15719.

de Haan, M. J., Brochier, T., Grün, S., Riehle, A., & Barthélemy, F. V. (2018). Real-time visuomotor behavior and electrophysiology recording setup for use with humans and monkeys. J. Neurophysiol. *120*, 539–552.

Dehnen, G., Kehl, M. S., Darcher, A., Müller, T. T., Macke, J. H., Borger, V., Surges, R., & Mormann, F. (2021). Duplicate Detection of Spike Events: A Relevant Problem in Human Single-Unit Recordings. Brain Sciences *11*, 761.

Delorme, A., Sejnowski, T., & Makeig, S. (2007). Enhanced detection of artifacts in EEG data using higher-order statistics and independent component analysis. Neuroimage *34*, 1443–1449.

Denker, M., Yegenoglu, A., & Grün, S. (2018a). Collaborative HPC-enabled workflows on the HBP Collaboratory using the Elephant framework. In Neuroinformatics 2018, p. P19.

Denker, M., Zehl, L., Kilavik, B. E., Diesmann, M., Brochier, T., Riehle, A., & Grün, S. (2018b). LFP beta amplitude is linked to mesoscopic spatio-temporal phase patterns. Sci. Rep. *8*, 1–21.

Fabietti, M., Mahmud, M., Lotfi, A., Averna, A., Gugganmos, D., Nudo, R., & Chiappalone, M. (2020). Neural Network-based Artifact Detection in Local Field Potentials Recorded from Chronically Implanted Neural Probes. In 2020 International Joint Conference on Neural Networks (IJCNN), pp. 1–8. (Glasgow, United Kingdom: IEEE).

Farina, D., Merletti, R., Indino, B., & Graven-Nielsen, T. (2004). Surface EMG Crosstalk Evaluated from Experimental Recordings and Simulated Signals: Reflections on Crosstalk Interpretation, Quantification and Reduction. Methods of Information in Medicine *43*, 30–35.

Georgopoulos, A., Kalaska, J., Caminiti, R., & Massey, J. (1982). On the relations between the direction of two-dimensional arm movements and cell discharge in primate motor cortex. J. Neurosci. *11*, 1527–1537.

Grün, S. (2009). Data-driven significance estimation of precise spike correlation. J. Neurophysiol. *101*, 1126–1140.

Grün, S., Abeles, M., & Diesmann, M. (2008). Impact of higher-order correlations on coincidence distributions of massively parallel data. In Lecture Notes in Computer Science, 'Dynamic Brain - from Neural Spikes to Behaviors', vol. 5286.

Grün, S., Diesmann, M., & Aertsen, A. (2002a). Unitary events in multiple single-neuron spiking activity: I. detection and significance. Neural Comput. *14*, 43–80.

Grün, S., Diesmann, M., & Aertsen, A. (2002b). Unitary events in multiple single-neuron spiking activity: II. nonstationary data. Neural Comput. *14*, 81–119.

Grün, S., Diesmann, M., Grammont, F., Riehle, A., & Aertsen, A. (1999). Detecting unitary events without discretization of time. J. Neurosci. Methods. *94*, 67–79.

Grün, S. & Rotter, S. eds. (2010). Analysis of Parallel Spike Trains. (Springer).

Harris, K. D., Quiroga, R. Q., Freeman, J., & Smith, S. L. (2016). Improving data quality in neuronal population recordings. Nat. Neurosci. *19*, 1165–1174.

Henze, D., Borhegyi, Z., Csicsvari, J.and Mamiya, A., Harris, K., & Buzsaki, G. (2000). Intracellular features predicted by extracellular recordings in the hippocampus in vivo. J. Neurophysiol. *1*, 390–400.

Hotelling, H. (1936). Relations between two sets of variates. Biometrika *28*, 321–377.

Islam, M. K., Rastegarnia, A., Nguyen, A. T., & Yang, Z. (2014). Artifact characterization and removal for in vivo neural recording. J. Neurosci. Methods. *226*, 110–123.

Jain, A., Kleinjohann, A., Graff, S., Doerenkamp, K., Kampa, B., Grün, S., & Musall, S. (2022). An adaptive analysis pipeline for automated denoising and evaluation of high-density electrophysiological recordings. 17 Mar 2022 - 20 Mar 2022, Lisbon(Portugal).

Jun, J. J., Steinmetz, N. A., Siegle, J. H., Denman, D. J., Bauza, M., Barbarits, B., Lee, A. K., Anastassiou, C. A., Andrei, A., Aydın, Ç., et al. (2017). Fully integrated silicon probes for high-density recording of neural activity. Nature *551*, 232–236.

Kilner, J. M., Baker, S. N., & Lemon, R. N. (2002). A novel algorithm to remove electrical cross-talk between surface EMG recordings and its application to the measurement of short-term synchronisation in humans. J. Physiol. *538*, 919–930.

Koh, T. J. & Grabiner, M. D. (1993). Evaluation of methods to minimize cross talk in surface electromyography. Journal of Biomechanics *26*, 151–157.

König, P., Engel, A. K., Roelfsema, P. R., & Singer, W. (1995). How precise is neuronal synchronization. Neural Comput. *7*, 469–485.

Ludwig, K. A., Miriani, R. M., Langhals, N. B., Joseph, M. D., Anderson, D. J., & Kipke, D. R. (2009). Using a Common Average Reference to Improve Cortical Neuron Recordings From Microelectrode Arrays. J. Neurophysiol. *101*, 1679–1689.

Morales-Gregorio, A., Kurth, A. C., Ito, J., Kleinjohann, A., Barthélemy, F. V., Brochier, T., Grün, S., & Van Albada, S. J. (2023). Neural manifolds in V1 change with top-down signals from V4 targeting the foveal region. BioRxiv .

Mumtaz, W., Rasheed, S., & Irfan, A. (2021). Review of challenges associated with the EEG artifact removal methods. Biomedical Signal Processing and Control *68*, 102741.

Musial, P., Baker, S., Gerstein, G., King, E., & Keating, J. (2002). Signal-to-noise ratio improvement in multiple electrode recording. J. Neurosci. Methods. *115*, 29–43.

Mölder, F., Jablonski, K., Letcher, B., Hall, M., Tomkins-Tinch, C., Sochat, V., Forster, J., Lee, S., Twardziok, S., Kanitz, A., et al. (2021). Sustainable data analysis with snakemake [version 1; peer review: 1 approved, 1 approved with reservations]. F1000Research *10*.

Nagaoka, T., Walker, D., Seaba, P. J., & Yamada, T. (1992). "Cross-talk" in recording evoked potentials. Electroencephalography and Clinical Neurophysiology/Evoked Potentials Section *84*, 473–476.

Nelson, M. J., Valtcheva, S., & Venance, L. (2017). Magnitude and behavior of cross-talk effects in multichannel electrophysiology experiments. J. Neurophysiol. *118*, 574–594.

Oberste-Frielinghaus, J. (2022). Baseline and Functional Correlations in Vision for Action Experiment. Master's thesis, RWTH Aachen University.

Pachitariu, M., Sridhar, S., & Stringer, C. (2023). Solving the spike sorting problem with kilosort. BioRxiv .

Perez-Prieto, N., Rodriguez-Vazquez, A., Alvarez-Dolado, M., & Delgado-Restituto, M. (2021). A 32-Channel Time-Multiplexed Artifact-Aware Neural Recording System. IEEE. Trans. Biomed. Circuits Syst. *15*, 960–977.

Pérez-Prieto, N. & Delgado-Restituto, M. (2021). Recording Strategies for High Channel Count, Densely Spaced Microelectrode Arrays. Front. Neurosci. *15*, 681085.

Quiroga, R. Q. (2007). Spike sorting. Scholarpedia J. *2*, 3583.

Rey, H. G., Pedreira, C., & Quian Quiroga, R. (2015). Past, present and future of spike sorting techniques. Brain Res. Bull. *119*, 106–117.

Riehle, A., Grün, S., Diesmann, M., & Aertsen, A. (1997). Spike synchronization and rate modulation differentially involved in motor cortical function. Science *278*, 1950–1953.

Riehle, A., Wirtssohn, S., Grün, S., & Brochier, T. (2013). Mapping the spatio-temporal structure of motor cortical LFP and spiking activities during reach-to-grasp movements. Front. Neural Circuits *7*, 48.

Rong, F. & Contreras-Vidal, J. L. (2006). Magnetoencephalographic artifact identification and automatic removal based on independent component analysis and categorization approaches. J. Neurosci. Methods. *157*, 337–354.

Rubino, D., Robbins, K. A., & Hatsopoulos, N. G. (2006). Propagating waves mediate information transfer in the motor cortex. Nat. Neurosci. *9*, 1549–1557.

Semedo, J. D., Jasper, A. I., Zandvakili, A., Krishna, A., Aschner, A., Machens, C. K., Kohn, A., & Yu, B. M. (2022). Feedforward and feedback interactions between visual cortical areas use different population activity patterns. Nat. Commun. *13*, 1099.

Shackman, A. J., McMenamin, B. W., Slagter, H. A., Maxwell, J. S., Greischar, L. L., & Davidson, R. J. (2009). Electromyogenic Artifacts and Electroencephalographic Inferences. Brain Topogr. *22*, 7–12.

Shu, Y., Duque, A., Yu, Y., Haider, B., & McCormick, D. A. (2007). Properties of action-potential initiation in neocortical pyramidal cells: Evidence from whole cell axon recordings. J. Neurophysiol. *97*, 746–760. PMID: 17093120.

Snyder, A. C., Yu, B. M., & Smith, M. A. (2021). A Stable Population Code for Attention in Prefrontal Cortex Leads a Dynamic Attention Code in Visual Cortex. J. Neurosci. *41*, 9163–9176.

Steinmetz, N. A., Aydin, C., Lebedeva, A., Okun, M., Pachitariu, M., Bauza, M., Beau, M., Bhagat, J., Böhm, C., Broux, M., et al. (2021). Neuropixels 2.0: A miniaturized high-density probe for stable, long-term brain recordings. Science *372*, eabf4588.

Stella, A., Bouss, P., Palm, G., & Grün, S. (2022). Comparing surrogates to evaluate precisely timed higher-order spike correlations. eNeuro *9*, ENEURO.0505–21.2022.

Stevenson, I. H. & Kording, K. P. (2011). How advances in neural recording affect data analysis. Nat. Neurosci. *14*, 139–142.

Torre, E., Picado-Muiño, D., Denker, M., Borgelt, C., & Grün, S. (2013). Statistical evaluation of synchronous spike patterns extracted by frequent item set mining. Front. Comput. Neurosci. *7*, 132.

Torre, E., Quaglio, P., Denker, M., Brochier, T., Riehle, A., & Grün, S. (2016). Synchronous spike patterns in macaque motor cortex during an instructed-delay reach-to-grasp task. J. Neurosci. *36*, 8329–8340.

Wim De Clercq, Vergult, A., Vanrumste, B., Van Paesschen, W., & Van Huffel, S. (2006). Canonical Correlation Analysis Applied to Remove Muscle Artifacts From the Electroencephalogram. IEEE Trans. Biomed. Eng. *53*, 2583–2587.

Yu, B. M., Cunningham, J. P., Santhanam, G., Ryu, S. I., Shenoy, K. V., & Sahani, M. (2009). Gaussian-Process Factor Analysis for Low-Dimensional Single-Trial Analysis of Neural Population Activity. J. Neurophysiol. *102*, 614–635.

Supplementary Material

Complexity distribution after removing all synchronous spikes

We examine the effect of the naive approach to remove all HSEs from the spike trains as proposed in Torre et al. (2016). Therefore we calculate the complexity distribution for the data after all spikes in HSEs are removed and compare this to the surrogates obtained from the data after the removal of the spikes. As to be expected, the distribution for the original data after the removal only contains entries for complexities of zero and one. However in the surrogates we find complexity up to six in the surrogate data, concluding that the data after removal significantly lacks synchrony since a certain amount of HSEs is expected. This shows that the naive approach should not be taken to remove synchrofacts.

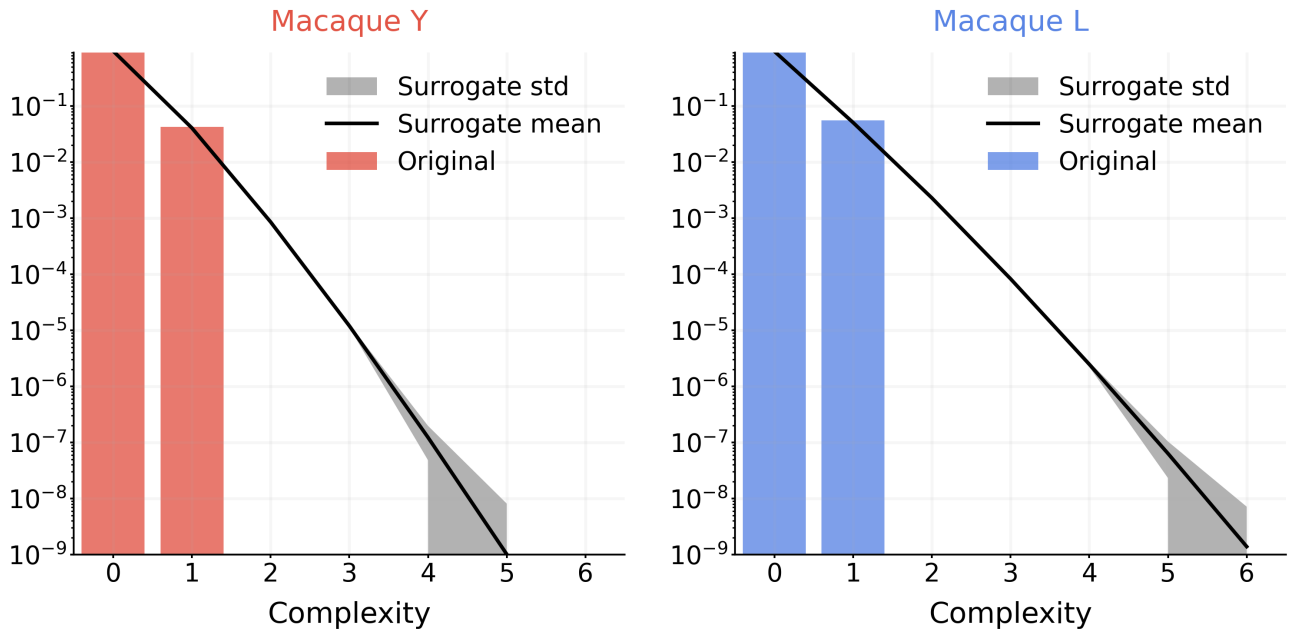

Figure S1: Complexity distribution after removing all synchronous spikes, Complexity distribution of the original data (colored bars), and the mean and standard deviation (line and shade, respectively) for the complexity distribution of the respective surrogates, $\frac{1}{30}$ ms bin size.

Connector mapping versus array mapping

In search for causes of strong raw signal correlations between channels, we examine the spatial distribution of the channels showing strong correlations on two spatial maps of channels: one on the level of the electrode arrays and the other the head stage connectors. In the case of macaque Y, the relative positions of channels are almost identical between the two maps, and hence we cannot conclude on which level the cross-talk is localized. In the case of macaque L, however, the spatial distribution of highly correlated channels is largely different between the array mapping and the connector mapping, indicating that the cause of the high correlations is localized on the level of the electrode arrays.

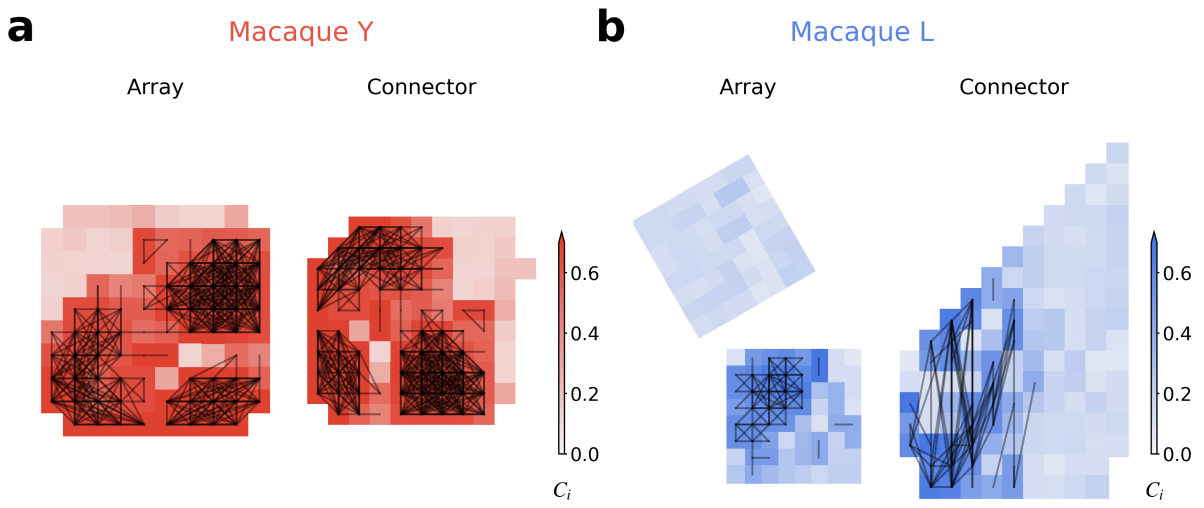

Figure S2: Comparison of spatial distribution of maximal raw signal correlation per channel (C_i) on the electrode array layout (left) and the headstage connector layout (right) for (a) macaque Y and (b) macaque L. Black lines connect electrode pairs with pairwise raw signal correlations $c_{i,j} > 0.4$.

Comparison between empirical and surrogate HSE index

To examine how large the HSE indices obtained from real data are in comparison to those from independent spike trains with matched firing rates, we plot the empirical pairwise HSE indices in the macaque Y data against the respective surrogate HSE indices obtained from time shifted surrogate data (Figure S3a; the mean over 200 surrogates is taken for each channel pair). The majority of channel pairs show larger empirical HSE index values than the respective surrogate values. This could reflect a bias originating from the definition of the HSE index that synchrofacts in channels with small numbers of spikes can be over-represented in the index. Hence, we next focus only on channels with firing rates greater than 1 spikes/s (Figure S3b). While a certain amount of channel pairs with large empirical HSE indices were screened out by this conditioning, we still see a considerable number of channels with extremely large empirical HSE indices compared to the surrogates, which are most likely the ones suffering from the cross-talk. After applying our proposed channel exclusion methods (Figure S3c and d), those channel pairs are screened out and the remaining ones show empirical HSE indices comparable to the surrogate indices, meaning that the remaining channels have as many HSEs as in independent spike trains. The mean of the empirical HSEs indices over channel pairs is still slightly higher than the mean of the surrogate HSE indices, which is likely due to other causes of synchrofact than cross-talk. One of such causes is common external noise across channels. Spike-like events generated by such noise typically show waveforms dissimilar to real spike waveforms, and hence can be effectively excluded by spike sorting. To check whether that is actually the case, we plot the HSE indices for SUA pairs in the same manner as before (Figure S3e-g). Again, after applying our proposed methods, SUA pairs show only as many HSEs as in the surrogates, and in this case of SUA pairs, the mean empirical HSE index is much more consistent with the mean surrogate HSE index than in the case of channel pairs.

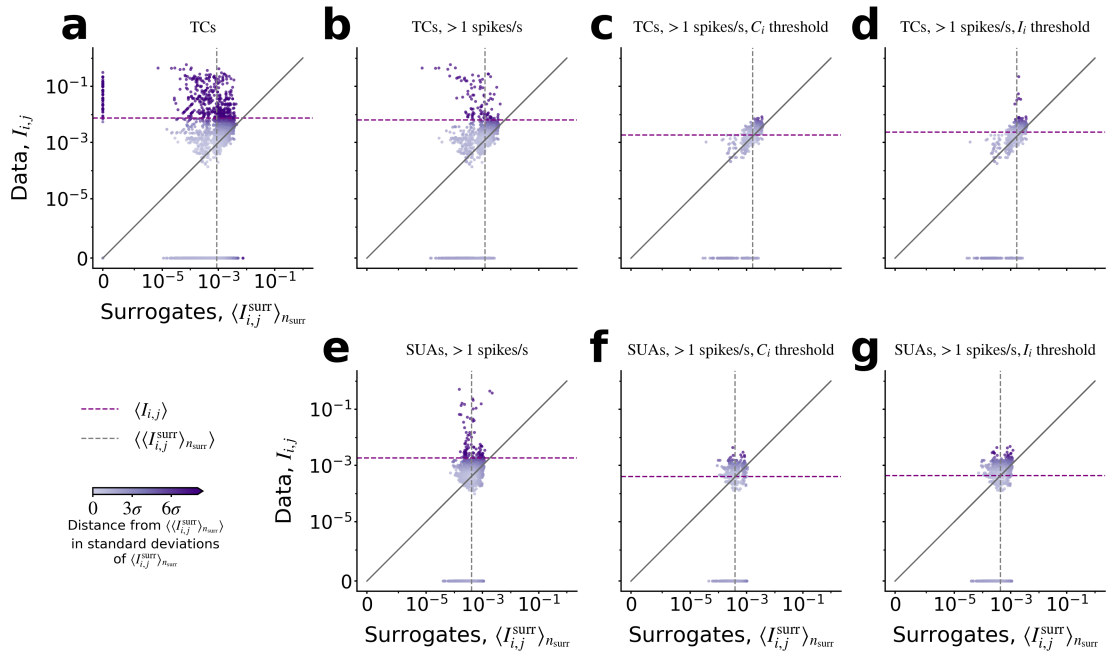

Figure S3: Comparison of the pairwise HSE index $I_{i,j}$ in the experimental data and the average of the corresponding surrogate data $\langle I_{i,j}^{\mathrm{surr}} \rangle_{n_{\mathrm{surr}}}$, each point corresponding to one channel pair. Mean of each variable is shown with a dashed line. The diagonal line indicates the identity between the two measures. The color shading represents the difference from the theoretically random data, at the point where the mean surrogate index $\langle \langle I_{i,j}^{\mathrm{surr}} \rangle_{n_{\mathrm{surr}}} \rangle$ crosses the diagonal; large deviations from this point are indicative of above-chance HSEs. The different panels show the results for the same session based on (a-d) all threshold crossings (TCs), or (e-g) spike sorted single units (SUAs). The different columns show different removal methods: (b, e) threshold on the firing rate, (c, f) threshold on firing rate and maximum cross-correlation C_i, and (d, g) threshold on firing rate and global HSE index I_i.

Common noise artifact example

The data of monkey L contained yet other feature in the data lasting about 500ms (see Figure S4, bottom) which can even be seen by eye. We identified this burst of synchronous spike activity as artifacts since these synchronous spikes also still exist on the sampling rate resolution (top). It introduced in the complexity distribution a huge amount of high complex events up to complexities of 35, which were still ubiquitous after our removal procedure. Such events did not exist in the data of monkey Y. Therefore we did cut out this piece of data before we further analyzed the data set for artifacts as we did for monkey Y. Monkey Y did not show any of these types of events.

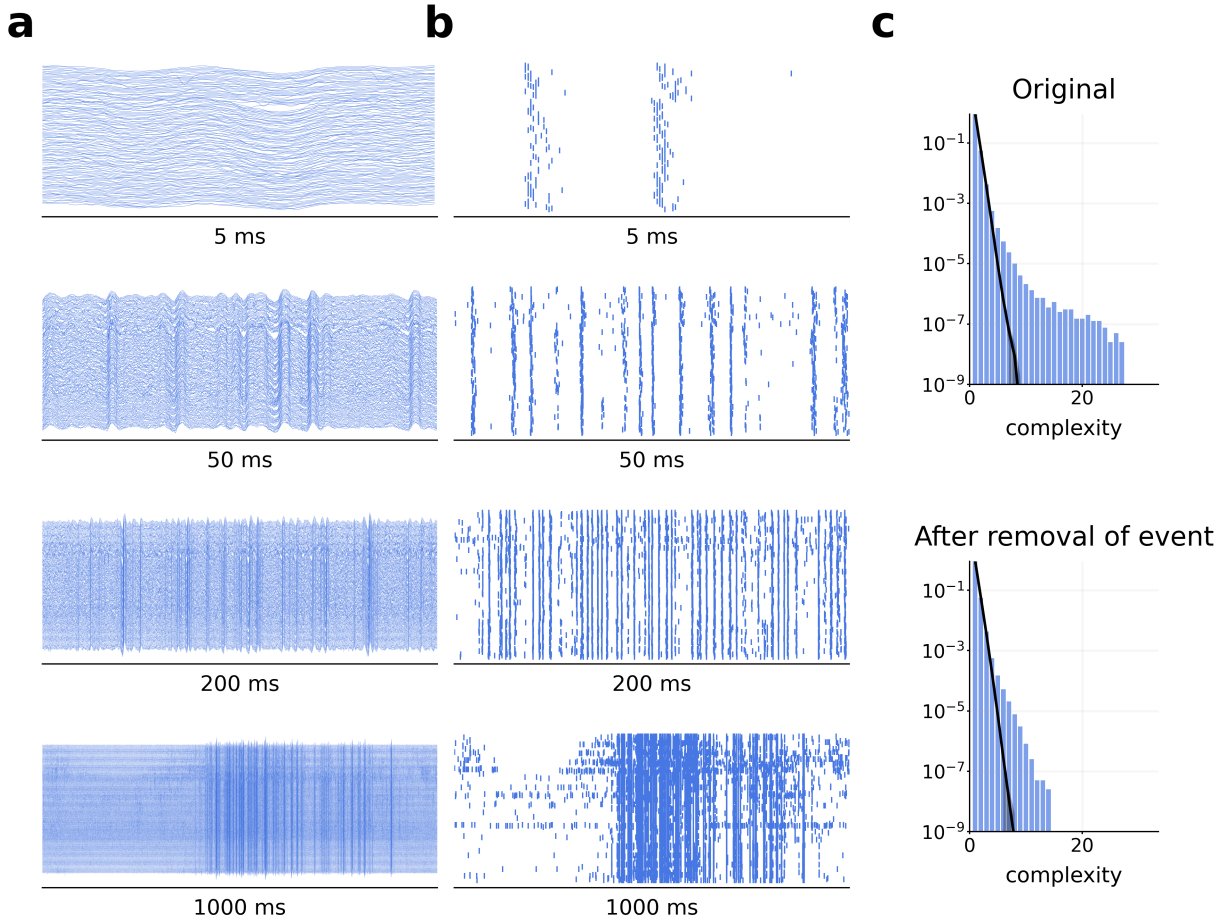

Figure S4: Burst artifact in monkey L. The left column, bottom shows the whole burst artifact, that expresses a lot of synchrofacts (on sampling rate of f=30kHz) one after the other over a period of about 500ms. The plots above show higher resolutions of that event, and on the top the total display shows piece of the data lasting 5ms. On the right top, the complexity distribution of the whole data set is shown, below after the complete removal of this burst event, which still contains artifacts. But as shown in Fig. 5 these can be completely removed by our removal procedure.